OBJECT IDENTIFICATION APPROACH FOR HYPERSPECTRAL AND MULTISPECTRAL THERMAL DATA

Thesis submitted to the Andhra University, Visakhapatnam in partial fulfilment of the requirement for the award of *Master of Technology in Remote Sensing and GIS*

Submitted By:

Richa Marwaha
M.Tech (Remote Sensing and GIS)
Photogrammetry and Remote Sensing
Department

Supervised By:

Dr. Anil Kumar
Scientist-'SF'
Photogrammetry and Remote Sensing
Department

Indian Institute of Remote Sensing, ISRO,

Dept. of Space, Govt. of India Dehradun – 248001

Uttarakhand, India

June, 2015

Disclaimer

This work has been carried out in partial fulfilment of Masters in Technology program in Remote Sensing and Geographic Information System at Indian Institute of Remote Sensing, Dehradun, India. The author is solely responsible for the contents of the thesis.

CERTIFICATE

This is to certify that **Ms. Richa Marwaha** carried out the dissertation entitled "**Object identification approach for hyperspectral and multispectral thermal data**" in partial fulfilment of the requirements for the award of **M. Tech. in Remote Sensing and GIS**. This work has been carried out under the supervision of **Dr. Anil Kumar**, Scientist/Engineer-'SF', PRSD, Indian Institute of Remote Sensing, ISRO, Dehradun, Uttarakhand, India.

…………………………..
(Anil Kumar)
Project Supervisor
Scientist-'SF'
Photogrammetry and Remote Sensing
Department

…………………………..   …………………………..
(Shefali Aggarwal)   **(Satya PS Khushwaha)**
Head, PRSD, IIRS   Dean (Academics), IIRS

DEDICATED TO MAA AND PAPA

ACKNOWLEDGEMENTS

DECLARATION

I, *Richa Marwaha*, hereby declare that this dissertation entitled "*Object identification approach for hyperspectral and multispectral thermal data*" submitted to Andhra University, Visakhapatnam in partial fulfilment of the requirements for the award of *M. Tech in Remote Sensing and GIS*, is my own work and that to the best of my knowledge and belief. It is a record of original research carried out by me under the guidance and supervision of *Dr. Anil Kumar*, Scientist/Engineer 'SF', PRSD, Indian Institute of Remote Sensing, Dehradun. It contains no material previously published or written by another person nor material which to a substantial extent has been accepted for the award of any other degree or diploma of the university or other institute of higher learning, except where due acknowledgment has been made in the text.

Place: Dehradun   Richa Marwaha

Date: 16th June, 2015

ABSTRACT

Landuse / Landcover (LULC) is important for natural resource monitoring. Landcover consists of various natural and man-made features present on earth's surface. Landcover mapping using high resolution data is advantageous in applications such as mineral mapping, resource management etc. As human activities are continuously affecting the environment at an unprecedented scale and speed, hence monitoring of landcover is a necessity. "Hyperspectral data" has high spectral resolution handling both difficulties and opportunities for LULC mapping. The primary objective of this paper is to find out best pixel-based and object-based algorithm for classification of thermal data and also to perform a comparative analysis of both the approaches. Minimum noise fraction (MNF) has been applied to thermal hyperspectral data and eight pixel-based classifiers (Constrained energy minimisation, Adaptive coherence estimator, Matched filter, Spectral angle mapper, Mixture-tuned matched filter, Target-constrained interference matched filter, Mixture-tuned Target-constrained interference matched filter and Orthogonal subspace projection) were tested. Similarly, segmentation was performed on thermal data and then, support vector machine (SVM) with linear kernel was applied under object-oriented classification approach. The best algorithm in pixel-based category was found to be spectral angle mapper (SAM) technique for thermal data set. SVM was quite useful for thermal data with high accuracy at scale value of 83 and merge value of 90, whereas for the combination of thermal data with coloured digital photograph SVM gave good results at scale value of 82 and merge value of 90. The results showed that object-based classification approach is more useful for such a high resolution airborne thermal hyperspectral data. Various roofs which were not detected using pixel-based techniques were extracted using object-based approach. The pixel-based and object-based classifiers were tested for ASTER thermal data also. The results suggested that for thermal data classification object-based classification approach is better than pixel-based approaches.

Keywords: Landcover, Minimum Noise Fraction (MNF), Spectral Angle Mapper (SAM), Support Vector Machine (SVM), Hyperspectral thermal data, Multispectral thermal data.

TABLE OF CONTENTS

LIST OF FIGURES

LIST OF TABLES

1.   INTRODUCTION

This section provides introduction to the present research work. The background and motivation is given in section 1.1. The problem statement is presented in section 1.2. The research objectives and research questions are presented in section 1.2 and 1.4 respectively. Section 1.3 describes the major innovation in this study. The structure of thesis enlisting the chapters is provided in section 1.6.

1.1.   BACKGROUND AND MOTIVATION

Landuse/Landcover (LULC) is a term which forms a critical component (Yang et al., 2010) of worldwide environment. Landcover is composed of various natural and man-made features present on earth's surface. Comprehensively talking, landcover portrays the physical condition (Anderson et al., 1976) of earth's surface. The term landcover signifies the natural features (Singh and Singh, 2011) that are actually present on the surface of earth. In contrast, landuse is a term which indicates human employment (Anderson et al., 1976) of landcover i.e. illustrating the purpose for which the land is being used (Kumar, 2006). Mapping or classification of landcover is vital for earth's resource management and planning. Landcover classification using high spatial resolution remote sensing data is advantageous in earth observation applications such as mineral mapping, species segregation etc. As human activities are continuously affecting the environment at an unprecedented scale and speed, hence monitoring of landcover is a necessity (Duan et al., 2012). In recent years, LULC has been a standout amongst most active areas of research internationally. Presently, the usage of remote sensing techniques for landuse classification (or mapping) is an imperative research tool. Monitoring of landcover is necessary for detection of changes in resources, and analyzing it. With the development of satellite technology since 1960's, vast amount of remote sensing data is available especially for landcover mapping applications (Duan et al., 2012). Remote sensing is a multidisciplinary branch of science concerning various themes like geoscience, physics, computer science, etc. which is closely linked to domain of earth sciences (Xu, 2000). The expression "remote sensing" refers to the art and science of classifying, detecting, and quantifying an object on earth without coming into direct contact with it. This procedure includes the recognition and estimation of radiation of different wavelength reflected or transmitted from far off objects or materials, by which object may be distinguished and categorized by class/type, substance, and spatial distribution (Graham, 1999). Remote sensing technique measures the reflected or emitted electromagnetic radiation from objects on earth's surface. These radiations can be measured in any region of electromagnetic spectrum such as; infrared region (0.7 μm to 300 μm), visible region (400 nm to 700 nm), and microwave region (1mm to 1m) (Liew, 2001) using the technologies be it multispectral or hyperspectral remote sensing. The multispectral and hyperspectral sensors are constantly being exploited for various remote sensing applications like mineral mapping, forestry, water resources etc. as they contains the information corresponding to the reflected energy or emitted energy from the objects on earth's surface. The most recent and important application is classification as these sensors contains potential for efficient detection. Object detection refers to detection and identification of particular target that are concealed or camouflaged in a disorderly background. "Hyperspectral data" has high spectral resolution handling both difficulties and opportunities for LULC mapping.

Remote sensing data in the range from visible to short-wave infrared region are highly stable for material identification or detection in the daytime as it uses reflectance-based spectral signature. A thermal remote sensing system may also convey the same outcomes for object detection at night. In the long wave-infrared (LWIR) region i.e. 8-12 μm the sensors, whether multispectral or hyperspectral sensors

acquires the radiance spectrum of the objects on the earth. This emitted energy is proportional to the temperature and emissivity of the object. The thermal infrared data from the multispectral as well as hyperspectral sensor contains a wealth of information. However, thermal infrared data is much noisier than optical data. Hence, it is difficult to handle such a data. So, detection/classification using this thermal infrared data is a challenge. This research work deals with hyperspectral as well as multispectral thermal data for identification of objects i.e. man-made and natural objects in the imagery. There exists numerous algorithms for processing remote sensing data for LULC map generation, however the algorithm yielding best landuse/landcover map (LULC) is still a subject of research for thermal hyperspectral data.

1.1.1. HYPERSPECTRAL REMOTE SENSING

Hyperspectral sensors started developing in 1980's by scientists at the Jet Propulsion Laboratory (JPL). These instruments could capture data in narrow contiguous wavelength bands. The spectral plots could provide fine details of the absorption phenomenon also. This was considered as a major breakthrough in the field of remote sensing. Hyperspectral data are represented as a 3-D cube with spatial information as one axis and spectral information as other two axis (Short, 2005). Hyperspectral imaging also known as "imaging spectroscopy" contain narrow contiguous spectral bands providing the contiguous spectrum which helps in the detection of minerals, for crops and bathymetry etc. On the contrary, multispectral sensors capture wide discontiguous wavelength bands identifying only major features in the imagery (Wilson and Davis, 1998). Hyperspectral sensors are based upon the Fourier transform-infrared (FT-IR) spectrometer, while multispectral sensors are based upon band pass filters (Small and Zhang, 2002). The first vision to fly imaging spectrometer from aircraft and spacecraft and still get the laboratory like spectra was of Dr. Alexander F.H. Goetz (MacDonald et al., 2009). Hyperspectral is an appealing technique proving rich geometric and radiometric information. Hyperspectral imaging sensors collect more than 100 bands leading to continuous reflectance spectrum for every pixel in the image scene. These contiguous and narrow bands are the characteristic feature of hyperspectral data which allows in-depth assessment of earth surface features which would else be 'lost' in coarse bandwidths acquired using multispectral scanners (Govender et al., 2007). These advantages govern the preference of classification of airborne hyperspectral data for this research work.

1.1.2. THERMAL REMOTE SENSING

Thermal infrared remote sensing is quite an immature technique lacking sufficient research work and paucity of empirical knowledge. Thermal infrared remote sensing is linked to various other important domains which can lead to edge-cutting breakthroughs in global change and development. Thermal infrared images are difficult to interpret because of radiance contrast ambiguity (Foy et al., 2002). Thermal infrared sensors capture the emitted energy instead of reflected energy from the object. The emitted energy from the object depends upon the temperature and emissivity of the surface. "Emissivity" is defined as radiance divided by blackbody radiance at kinetic temperature. It depends on the physical properties of the object (Kirkland et al., 2002). So, certain surface information which was not captured using reflected data can be measured using thermal data. Thermal infrared data act as a complementary to reflective region but also a valuable tool in remote sensing applications (Project et al., 2000). Thermal infrared data has been used in war battlefield to actualize detection, identification and recognizing targets. The detection means differentiating the target from background, while orientation involves finding out the aspect of target whereas recognizing means assigning target to a class. Hence, target detection involves both detection as well as recognition of targets (Ratches et al., 2001). One such

application is search and rescue operation i.e. detection of airplane crashes within the natural background. This automatically detects the objects in the crash site. Hence, the airborne LWIR hyperspectral data was chosen for this research work.

1.2.   PROBLEM STATEMENT

The digital image classification using very high resolution image is generally a difficult task particularly for urban class (Wu et al., 2014). Diverse sorts of building materials gets mixed up with each other (Sims and Mesev, 2007). The landcover in this study is composed of asphalt roads, concrete and other similar type of materials. They have almost similar spectral signatures making it difficult to extract objects/classes using pixel-based classification techniques. Also, pixel-based classification techniques faces the problem of salt and pepper noise post-classification (Zheng et al., 2014). Hence, object-based was used as it took into account spectral, spatial and textural information (Zhang and Jia, 2014). Nonetheless, a potential weakness of object-based image analysis is the issue of over-segmentation, under-segmentation and spectrally similar classes (Zerrouki and Bouchaffra, 2014). In literature many segmentation algorithms exists such as mutli-resolution segmentation, and watershed segmentation. These algorithms iteratively groups the pixels based on some pre-defined similarity criteria which can be difficult to determine. Classification is then performed based on spectral, textural and spatial attributes. As a result, if segmentation is not good, then classification will not be reliable. As a result, a comparative study of image classification approaches for high resolution data has been presented. The objective of this paper is to compare the results obtained using pixel-based techniques versus object-based classification techniques for landcover mapping, particularly classification of various roof types. For this the developed methodology was tested for two types of sensors' data i.e. thermal multispectral data which has coarser resolution and airborne thermal hyperspectral data which has high spatial and spectral resolution. Earlier work, as shown in literature review have been performed for the optical imagery. Not much of the work have been carried out for this type of dataset. Hence, this research work was tested for classification of thermal infrared data. The main challenge here is in handling of a noisy and voluminous data for such an important application.

1.3.   RESEARCH OBJECTIVES

The primary objective of this research work was to establish and formulate a tested and acceptable methodology to extract object classes (like road, trees, red roof, grey roof, concrete roof, vegetation, bare soil etc.) from the study area, using airborne thermal hyperspectral data, and classes like urban area, forest, agricultural area, water and sand from multispectral thermal data. This also includes applying data dimensionality reduction (MNF) algorithms. The objectives of this research work were the following:

1. To apply data dimensionality reduction technique: minimum noise fraction i.e. MNF technique on airborne LWIR hyperspectral data.
2. To extract objects from airborne LWIR hyper-spectral data, from colored photograph with airborne LWIR hyper-spectral data and from ASTER thermal data using pixel-based classifiers.
3. To extract objects from airborne LWIR hyper-spectral data, from colored photograph with airborne LWIR hyper-spectral data and from ASTER thermal data using object-based classifiers and its comparison with pixel-based classifiers.

1.4. RESEARCH QUESTIONS

For the achievement of the research objectives this study made use of data dimensionality reduction techniques and use of various detection algorithms. For this reason the prime aim is to answer the following questions.

1. How MNF database will affect the results of object detection?
2. Which pixel-based classifier is best for extraction of each class?
3. Which object-based classifier is best-suited for extraction of each class?
4. Which approach is better: pixel-based or object-based technique?

1.5. INNOVATION

The innovation aimed at through this research was an attempt to utilize MNF technique and various target detection approaches for object identification from airborne thermal hyperspectral data and from multispectral thermal data. Also to study the implications of this method of data dimensionality reduction on accuracy of classification of object classes from the image. The study area is a combination of manmade and natural object classes. The innovation for this study is the use of pixel-based and object-based classification approach for thermal dataset.

1.6. STRUCTURE OF THESIS

This thesis is divided into 7 chapters as follows:

1. **Chapter one** presents an overview of landuse / landcover (LULC) concept and presents a brief insight into hyperspectral remote sensing and thermal remote sensing. The main objectives and research questions are also presented.
2. **Chapter two** deals with the literature review about different stages and various relevant aspects of the thesis is presented which includes most relevant work on dimensionality reduction methods, object detection and previous work on different object-based image analysis.
3. In **chapter three**, the mathematical concepts of the algorithms and techniques used are explained for better understanding of the theory.
4. The **fourth chapter** is divided into two sections providing detailed information regarding study area and the datasets used for the research work.
5. The methodology followed to carry out this study is depicted in **chapter five**. It describes detailed workflow of the research work. It is divided into three parts. The first part deals with the application of data dimensionality reduction approach on airborne LWIR hyperspectral data. The second part acknowledges the implementation of pixel-based classifiers on the datasets. Then, object-based classifiers used are detailed in third section.
6. The subsequent chapter following the methodology is results and discussion which is given in **chapter six**. The results for both pixel-based and object-based classifiers are discussed in this chapter.
7. The answers to research questions are presented in **chapter seven** concluding the research work. It also deals with the recommendations for the future research. The references corresponding to the literature followed and the appendix containing the publications are in subsequent chapters.

2.   LITERATURE REVIEW

This chapter deals with the detailed review of the relevant literature reviewed for this research work. The following sections substantiates the use of thermal hyperspectral and multispectral data, understanding of its dimensionality problem, choice of pixel-based and object-based detector and performance measures used in this research work.

2.1.   HYPERSPECTRAL REMOTE SENSING

This section deals with the understanding of hyperspectral imaging and the previous which have been done using this type of dataset. Hyperspectral imaging is also known as imaging spectroscopy. Imaging spectroscopy can be defined precisely as "The simultaneous acquisition of images in many narrow, contiguous spectral bands so that a continuous reflectance spectrum can be reconstructed for each picture element (pixel) in the scene" (Vane and Goetz, 1985).

Spectroscopy started with the advent of prism in late 1700's. Since then there is no looking back as there has been a rapid development in the optics. The main principle of hyperspectral imaging is that a detector i.e. charged coupled device (CCD) generates a spectrogram i.e. image as a function of colour. The sensor is also moved relative to the target to get the full spatial extent (Sigernes, 1996). Imaging spectroscopy started in early 70's. Hyperspectral images advanced with the digital electronics. "HYPER" literally means too much. This overabundant spectral information is a necessity to identify each material efficiently in any hostile environment. The hyperspectral imaging is beneficial over multispectral imaging because of the following reasons (Zhu et al., 2011) (Goetz, 2009):

1. Hyperspectral data have high spectral resolution.
2. It collects the data constantly in a distinct spectral range due to which it contains a wealth of spectral information.
3. Bands in hyperspectral data are contiguous and overlapping so that all the information is detected. The base point here is that the bands ought to be adjoining not the "number" of bands.
4. Contiguous spectrum assists to recognize atmospheric windows for its removal from radiance signal, which is not applicable for multispectral sensors.
5. SNR (signal to noise ratio) of data can be enhanced by comparing pixel spectral with reference which is not possible in case of multispectral data because of number of discontiguous sampling.
6. It can solve the problem of mixed spectra by directly deriving the relative abundance of materials.
7. The classes/objects in hyperspectral image can be analysed from various spaces: image space, spectral space, and character space.

As hyperspectral images possess high spectral resolution and low spatial resolution, so a single pixel may contain spectra from more than one material. Hence, separating each spectrum from the mixed pixel becomes an important issue. Chen et al., 2009 in his paper described a generalised technique of linear unmixing (Chen et al., 2009). To solve this problem a method called Endmember Extraction Algorithm (EEA) was used to separate each spectrum from the mixed pixel (Mozaffar et al., 2008). Since, the hypercube data contains massive information with overlapping bands. Hence, statistical analysis for 3-D hypercube becomes problematic. Traditional laboratory spectra collection is also a perplexing task. Brown, 2006 developed automatic process for investigation of hyperspectral data. This method detects

a small shift in wavelength and evaluate the physical properties of materials (Brown, 2006). The spectral information from VNIR to SWIR spectral region (400-2500nm) was used to assess the properties of urban materials. This spectral information from hyperspectral image (HSI) along with the geometrical information was combined together. This fused information was used to get 3-D structure and to detect the urban material (Brook et al., 2010).

Hyperspectral data is an exceptional material identifier. For fine detection of objects hyperspectral remote sensing is proving to be an ace by providing a rich database for different types of materials. It can sense the fine spectrum of objects on ground which remains undetected by wide band remote sensing approaches. One such challenge is in identifying building surface material using hyperspectral image. This is certainly a very new research area. Zhu et al., 2011 used spectral angle mapper (SAM) for object identification and developed an IDL program to identify building materials. The results achieved were quite satisfactory (Zhu et al., 2011).

Apart from material detection hyperspectral imaging is also used for the classification purpose. An oldest method of classification called k-nearest neighbour (k-NN) is unable to handle such a high dimensional dataset. So, Li et al., 2014 coupled k-nearest neighbour (k-NN) with the distance weighted Tikhonov regularization called nearest-regularised subspace (NRS) classifier (Li et al., 2014). Other method of classification included two different types of datasets i.e. hyperspectral data and DSM digital surface model data. An approach called improved binary encoding (IBE) was used which incorporated both pixel-based as well as object-based techniques. Accuracy of about 95% was achieved (Xie et al., 2009). For earth observation applications the role of hyperspectral data is quite noteworthy. Eradicating the band correlation in hyperspectral data and the limitations of various classifiers Du et al., 2009 established a decision-level fusion method. The accuracies obtained using this approach was found to be 92.67%, 96.86%, 90.65% and 93.33% for first, second, third and fourth scheme (Du et al., 2009). Kernel fisher discriminant analysis was used for classification of hyperspectral image which was quite efficient in terms of time taken for the computation. Its accuracy was comparable to the SVM i.e. support vector machine (Yang et al., 2007). Spacecraft based hyperspectral data contains high spectral information but lacks in high spatial resolution. So, Winter & Winter, 2002 described a method called joint endmember determination and unmixing, which used separate high spatial resolution imagery along with the hyperspectral imagery of high spectral information. Classification was performed exploiting both spectral and spatial information. Firstly automatic registration of two datasets was done. Then, for resolution enhancement two methods were used: colour product sharpening and hyperspectral data sharpening (Winter and Winter, 2002). Bochow et al., 2012 developed an algorithm using airborne hyperspectral image which was fully automated neither requiring training pixels nor any prior knowledge. This worked on any water type such as turbid water, lake water removing any type of shadow occurring in the image (Bochow et al., 2012). New automated method called Spectral overlapping threshold (SOT) used multistrip airborne hyperspectral data for change detection. It used algorithms such as – spectral angle measure (SAM), spectral information divergence (SID), Euclidean distance measure (ED) and spectral correlation measure (SCM) (Adar et al., 2014).

The purpose behind adopting hyperspectral imaging is incorporation of hundreds of narrow contiguous bands. Various materials show different spectral features. Certain plants and vegetation can be characterized by wide, slowly varying spectral features. In the same way materials, like minerals and gases, possess very narrow spectral features, and its location in the spectral band varies for each class of material. Subsequently, narrow wavebands are needed to resolve features that help to differentiate similar spectra. Contiguous bands are needed to detect materials, as imperative features may be in

diverse spectral locations for each material. Accordingly, if the interest was on just a couple of target materials and backgrounds, a predetermined number of precisely picked narrow bands would be adequate to recuperate the spectral features. Now, more and more number of bands would be necessary to discriminate the feature. The essence of hyperspectral processing is detection and identification of materials and the suppression of redundant or common features (Shaw and Burke, 2003).

As image is acquired in narrow bands, fine spectrum is obtained for each object. This opened up hyperspectral to many of the applications such as precision farming, monitoring invasive plant species, insects, and crop yield and so on (Teke et al., 2013). Hyperspectral data has incredible importance in agriculture management owing to the qualitative advantage of visual overview and qualitative assessment and monitoring (Mozaffar et al., 2008). These applications cover the range from visible to infrared range in electromagnetic spectrum. Hence, this justifies the use of hyperspectral dataset for this type of research work. Next section deals with the importance of airborne hyperspectral sensors owing to its both high spectral and spatial resolution.

2.2.   AIRBORNE SENSORS

Airborne sensors specifically hyperspectral sensors have existed for over two decades. Birk and McCord, 1994 presented a brief comparison of 19 airborne hyperspectral sensors elaborating the design, hardware properties and applications. The principle of airborne acquisition was also shown in this paper according to which scanning is done in the direction of X-axis whereas plane's forward motion provides the Y-axis. The imager inside the plane spits the light into many narrow channels on per pixel basis. Various scanning mechanisms for earth coverage are: scanning, staring, scanning/staring and staring arrays. One of the important parameter to gauge the performance of the airborne sensor is SNR i.e. signal to noise ratio. For exploitation of this type of data for better earth observation, data acquisition and data processing techniques are being evolved (Birk and McCord, 1994).

Airborne sensors has an added advantage of less cost over space borne sensors but keeping in view the restriction of terrain and weather space borne sensors are increasingly used. But in order to cover up the cost of the space borne sensors various simulation approaches are being developed to simulate space borne image from airborne image (Zhang et al., 2008).

Along with the advantages airborne image suffers from various noises like stripe noise, random dead pixel and so on. These type of noise can seriously affect the processing and hence its results. So it becomes an important task to get rid of such anomalies. A method combining the strengths of two destriping method – calibration method and image static method is presented. This is a novel method applicable not only to hyperspectral but also to multispectral as well as panchromatic (Duan et al., 2013).

Sometimes a single classifier may not able to work up to the mark individually and each of the classifier has its own strength and weakness. So, Zhang et al., 2009 proposed a methodology combining the strengths of various algorithms and developed a method called Cumulative-Separation based (CSB) method to detect mines (Zhang et al., 2009). Henceforth, airborne hyperspectral sensors have many applications namely- mine detection, water delineation. One such application utilising this type of sensor is to find the river water quality assessment and its comparison with ground based sampling (Olmanson et al., 2013). Be it airborne or space borne hyperspectral imager, dimensionality reduction is of utmost importance. Its importance is described in next segment.

2.3.   DIMENSIONALITY REDUCTION

The effect of training samples is very important parameter in classification. As number of classes and number of spectral bands are very large then training samples must be equivalent. But such large number of training samples are expensive to collect and are time consuming. Hughes phenomenon is loss of classification accuracy when the dimension of data increases and the training samples remains same. So, to mitigate the effects of Hughes phenomenon, various data dimensionality reduction techniques are used (Shahshahani and Landgrebe, 1994). Vast amount of information is available in the hyperspectral images. But correct handling and exploitation of this data is important and interesting task (Wang et al., 2012). Dimensionality reduction refers to transforming the data from high dimension space to lower dimensional space while preserving information of interest. Data dimensionality reduction is significant in case of huge data sets like hyperspectral data so as to reduce computational complexity and improve accuracy. To combat the curse of dimensionality many techniques are available**.** There are two approaches to accomplish this task i.e. feature extraction in which original character of information is distorted and band selection method which preserves the original information.

Intrinsic dimensionality is the smallest dimensionality which represents two-dimension distribution of data in three-dimension. Linear analysis method utilises feature space distribution and statistical methods to find to transform data into linear structure to find the intrinsic dimensionality of the hyperspectral data. Some of the linear projection methods are PCA (principal component analysis), ICA (independent component analysis) and PP (projection pursuit). These techniques are not much efficient as they do not exploit all the information present in the data. Hence, some of the non-linear projection methods nullify the disadvantages of the linear approaches. Non-linear method replaces the intrinsic dimensionality with the lower dimension data. Non-linear techniques for projection are non-linear multidimensional scaling, Sammon's non-linear mapping and Kohonen self-organising maps (Lennon et al., 2002). Many factors make analysis of HIS data difficult and hard task calling for sophisticated methods and algorithm. An important issue is extremely high dimension and size of data because of high spatial, spectral, temporal resolution. Some methods of feature extraction are PCA, MNF and spectral based approach i.e. DWT discrete wavelet transform. Feature extraction methods are based on distance metrics, Euclidian mutual information, and Bhattacharya distance (Bioucas-dias et al., 2013).

One of the most famous and widely used approaches for dimensionality reduction is PCA i.e. principal component analysis. It is a linear projection method. It decorrelates the bands in the data and removes the redundancy apart from the advantages; some of the disadvantages of this transform are that it is time consuming and does not preserve the local spectral features. This may degrade the quality of classification (Kaewpijit et al., 2002). A new technique called Bandlet transform is also an efficient method that can be used for the reduction of dimension. Firstly the image is segmented using quad tree segmentation algorithm then bandlet coefficients are found. These coefficients are replaced by the first principal component. Then inverse bandlet transformed is applied to get the transformed output image (Du et al., 2013). A higher level technique called kernel independent component analysis (KICA) is much useful approach which is superior to ICA i.e. independent component analysis. KICA is a robust technique which is a non-linear method and works even with Gaussian data (Khan et al., 2009).

2.4.   PIXEL-BASED CLASSIFICATION

Target detection is a two class classification problem known as binary classification and it focuses on maximizing the probability of detection (Du and Zhang, 2014; Zhang et al., 2014) with low false alarm

rate. Anomaly detection is defined as "The pixels deviating from the background are identified as target pixels which can be calculated using statistical model of the background". To realize this condition the statistical model of background was considered such that it is represented by sum of multivariate normal probability distributions. The parameters of this model are estimated using stochastic expectation maximisation (SEM). It was found that performance increases with the number of distribution components (Kasen et al., 2004). Traditional target detection methods are based on the fact that the target and background pixels in the image are pure pixels which do not happen practically. Hence those methods are purely based on the fixed distance measurement. Du et al., 2013 portrayed a robust and efficient algorithm called Unsupervised transfer learning based target detection i.e. UTLD which follows three steps as under:

1. Multivariate outlier analysis: Automatically choosing the positive and negative samples i.e. target and background pixels. So, a mean and covariance matrix is generated using the background pixels. New threshold is set using the Mahalanobis distance of the matrix.
2. Segmentation method: It is used to get the unlabelled samples. Graph-based technique is used to segment the image. Image is segment to get homogeneous regions.
3. Subspace is constructed using a transfer learning method (Du et al., 2013).

Also, Multi-detector strategy is adopted which involves fusion of many detection algorithms. Dynamic subspace detection (DSD) algorithm is used which creates the subspace separating the targets and on-target pixels (Du and Zhang, 2014). Very less work has been done in the field of improving the accuracy via band selection for target detection (Wang et al., 2012). Lefei Zhang et al., 2014 introduced a feature extraction algorithm called Sparse Transfer Manifold Embedding (STME) for target detection. It works well even when the training samples are sparse. It is machine learning dimensionality reduction method. Its performance can be evaluated using ROC receiver operating characteristics and FAR i.e. false alarm rate (Zhang et al., 2014).

A broadband array spectrograph system (BASS) mounted on a military vehicle which is a non-imager sensor. This is mounted on a military vehicle collecting hyperspectral data in LWIR (8-13 µm) range. Spectral indices of vehicles, sand and limestone are calculated from in-scene data. These indices are then applied to the data collected by BASS instrument. This can detect the military vehicle at any time day or night. SNR of over 1000 is sufficient for the detection (Bongiovi et al., 1998).

A brief introduction of the architecture and the demonstrator of the airborne real time target detection were exhibited in the paper written by Haavardsholm et al., 2010. This system uses HySpex VNIR-1600 HS camera while the demonstrator is built in C++ language and is a cross platform framework. This demonstrates the real time target detection (Haavardsholm et al., 2010). Bar et al., 2010 presented a robust algorithm combining both spatial and spectral analysis. As the hyperspectral image suffers from the poor spatial resolution hence a high resolution imagers is used which aids the high resolution analysis. A detection technique is shown in this paper which works in two steps: anomaly detection and classification. At the spectral detection step there is high probability of detection while at spatial step false alarms are reduced. The algorithm was tested for various landscapes and various terrains (Bar et al., 2010). Ratches, 2011 provided the insight into the current aided/automatic target acquisition technology for the military work. In this paper AiTR i.e. aided/automatic target recognition is defined as "A fully automated process performed on the imaging data to carry out functions ranging from simple to more complex functions." The veracity of AiTR lies in the fact that it provides massive functionalities to the soldier in the warfare. This algorithm accomplishes following functions:

1. Pre-processing of hyperspectral image i.e. noise removal, correction of bad pixels etc.
2. Detection: target detection, anomaly detection.
3. Information extraction: spectral features, spatial features, temporal features.
4. Classification (Ratches, 2011)

Target location is also very crucial in the field of Infrared Search and Task (IRST). Ying et al., 2003 used wavelet multiresolution edge detection algorithm for detection. This algorithm searches for a potential area in which the target is present. Using least square fitting a line equation is established. Edge detection procedure is used to find the sea-level line. Wavelet transform has an advantage of local analysis in spatial and frequency domain. Wavelet transform has ability to work in the noisy image as decomposed images are not distorted. Another function called as Mutual Wavelet Energy Combination (MWEC) eliminates the background clutter. So, overall this algorithm works well for small target, low contrast and noisy image (Ying et al., 2003).

Cho et al., 2009 carried out a study aimed at discriminating various tree species using multiple endmembers spectral angle mapper (SAM) approach. This technique was compared with the single endmember spectral angle mapper (SAM) approach. In this work spectral reflectance of each of the species' leaves were uses to validate this approach. This research showed that there is 60% increase in overall accuracy using multi-endmember SAM than using single-endmember SAM approach (Cho et al., 2009). SAM i.e. spectral angle mapper technique was also used to separate the healthy and contaminated corn kernels. Fluorescence images were used for this research work. Spectral angle mapper (SAM) was used as the effect of illumination is very low on this. Based on the given threshold classification was performed. For 20 ppb, accuracy of 86.1% and for 100ppb, accuracy of 88.1% was achieved. In this intensity of fluorescence was ignored which is an important part of the image (Yao et al., 2010). As spectral angle mapper (SAM) is unable to handle non-linear data with overlapping classes, hence a non-linear approach called kernel spectral angle mapper (SAM) was used. This technique was tested for Beijing-1 satellite's multispectral images. The results showed that the accuracy increases by using kernel SAM method. It was further suggested to use mixture kernels for better image classification (Liu and Yang, 2013).

Tiwari et al., 2013 compared the spectral matching algorithm, spectral anomaly detection algorithm with the independent component analysis (ICA). Four spectral matching algorithms are OSP (orthogonal subspace projection), CEM (constrained energy minimisation), SAM (spectral angle mapper) and SCM (spectral correlation method). Anomaly detection methods are OSPAD (orthogonal subspace anomaly detector), RX anomaly detector, UTD (uniform target detector) and RXD-UTD. These techniques were tested for AVIRIS data and synthetic data. Anomaly detectors did not perform well for AVIRIS data. ICA outperformed both spectral matching and anomaly detectors. ICA hence, proved to be an alternative to all these algorithms (Tiwari et al., 2013).

The strength of target detection lies in the fact that there should be more disparity between target-embedded mixed spectrum and the background-spectrum. Two measures are used to evaluate the performance of the algorithm which is (1) target-to-clutter-ratio TCRs[2], (2) receiver operating characteristic curve ROC

TCRs[2] is a measure of distinction between target and background and is given by equation 2.1:

$$TCR^2 = \frac{(\Delta L)^2}{\left[\frac{(n_T-1)\sigma_T^2+(n_B-1)\sigma_B^2}{n_T+n_B-2}\right]} \tag{2.1}$$

Where, n_T and n_B = number of samples in target and background class respectively.

σ_T and σ_B = target and background samples standard deviations.

ΔL = Difference between mean signature of background and target class.

ROC curve quantifies probability of detection (Pd) vs probability of false alarm (Pfa). High value of Pd and low value of Pfa means good target detection (Luo et al., 2007).

There are various applications of target detection techniques. Target detection in hyperspectral imagery is utilised in both fields-military and civilian applications. Civilian applications comprise of sea detection, applications in urban and geology, ocean remote sensing, vegetation surveys and environmental modelling etc. Military applications include target reconnaissance, camouflage, anti-camouflage, battle damage assessment, providing enhancement s to weapon operator and surveillance etc. (Zhu et al., 2011) (Wang et al., 2012) (Ratches, 2011).

The key challenge thwarting the progress of target detection technique is level of false alarm in real environment (Ratches, 2011). Major problem in target detection is characterisation of covariance matrix for target as well as background with limited training samples (Bioucas-dias et al., 2013). So, to fill the gaps in the study and based on the previous work done, eight algorithms (explained in the section 5 methodology) for target detection were chosen for this study. These helped to mitigate the glitches in the existing algorithms.

2.5.   OBJECT-BASED CLASSIFICATION

Object-based classification approach was used for classification of high resolution imagery with the help of digital line graph. The accuracy without the use of digital line graph was 0.789, whereas the accuracy with the use of digital line graph was 0.9578. This suggests the use of additional data for better object-based classification (Sims and Mesev, 2007). Zheng et al. proposed the use of contextual information for noise removal from the pixel-based results. The salt and pepper noise which is produced after classification by pixel-based methods was removed using post classification smoothing and object-based classification (Zheng et al., 2014). The combination of pixel and object based approach was used in the study conducted in urban area with IKONOS imagery. First of all pixel-based classification was performed and then, segmentation was done to further improve the classification. Hence, a more detailed classification map was produced (Shackelford and Davis, 2003). For object-based classification four classification approaches were used such as maximum likelihood classification, use of mean spectral values with MLC, nearest neighbour classifier and separability and thresholding algorithm. The highest accuracy was obtained with classifier utilizing both spectral and spatial information (Gao et al., 2003). A new approach for object-based classification was used. First of all image was segmented and texture and morphology were extracted from it. It was stacked with the original image and maximum likelihood classification was performed. The results suggests that the inclusion of spatial information increases overall accuracy (Salehi et al., 2011). An approach for classification of high resolution imagery was performed in a work by Yu et al., 2006. The classification was augmented with the topographic data.

Fractal net evolution method was used for segmentation. Nearest neighbour classification technique was used for classification. For comparison with pixel-based classification maximum likelihood classification approach was used. This led to the conclusion that spatial information helps in increasing accuracy (Yu et al., 2006). A study for finding optimum segmentation parameters was conducted by Darwish et al. Multi-resolution segmentation was used. The study was carried out on two datasets i.e. Landsat and IRS dataset. From the results analysis it was found that IRS produced better accuracy than Landsat (Darwish et al., 2003). The urban area classification using object-oriented classification approach was conducted by Kupková et al., 2009. The study was conducted on QuickBird dataset. The complexity of urban environment was reduced by dividing the urban area into homogeneous segments. The classification was carried out using fuzzy classification approach. From results it was found that this technique was not much useful for sub-urban areas (Kupková et al., 2009). Object-oriented classification for extraction of building between 2002 and 2010 was used by Tsai et al., 2011. In this two approaches were used on high spatial resolution data of QuickBird i.e. post classification and bi-temporal layerstack classification approaches. Two software's were used i.e. feature analyst and ENVI Feature Extraction software. From the analysis of results it was found that bi-temporal layerstack classification method was superior to post classification method. Also, feature analyst software was more useful than ENVI Feature extraction software (Tsai et al., 2011). For LULC classification WorldView-2 dataset was used by Zhou et al., 2012. For detailed classification object-oriented classification technique was adopted. First of all multi-scale segmentation was carried out. Then, feature selection and rule set was created. At last classification was carried out. It was found that object-oriented technique produced 79.4% accuracy. Also, producer accuracy was also found to be high (Zhou et al., 2012). The segmentation algorithm and classification algorithm is depicted in next sub-sections.

2.5.1. SEGMENTATION

Object-oriented classification technique involves two steps i.e. segmentation band classification. Image segmentation is an important part of object-oriented approach. Traditional segmentation approach involves segmenting the image into homogeneous segments. Here watershed algorithm was used for the segmentation purpose. Watershed algorithm works on a single gradient imagery. Gradient image is calculated using two methods i.e. edge detection and intensity detection methods. Edge detection uses Sobel edge detection method for computation of gradient image. The darker pixel in the gradient image is considered as a lowest elevation point called minima. It starts with minimum pixel value and partitions the image into regions with similar pixel intensities. Hence, segmented image is obtained.

WATERSHED ALGORITHM

A major application is in medical imaging. Considering the noise and over-segmentation problems in traditional watershed algorithm. A new technique was proposed in which independent component analysis was performed to reduce noise and reduce over-segmentation. Then, this image was given as input to watershed algorithm. This was quite efficient method (Zhang et al., 2012). Another method was proposed in which, first of all K-mean clustering was used for segmentation and then, watershed algorithm was used for further segmentation. This improved the accuracy of the results (Ng et al., 2006). One more application of watershed algorithm in medical domain was separation of each tooth from X-ray image. Watershed was combined with the mathematical morphology. Morphology enhances the images. The contrast was improved and noise was removed using top-hat-bottom-hat transformation. Erosion procedure helps in weakening the adhesion between teeth. Hence, watershed algorithm was applied to the transformed image. This proved to be an efficient method (Li et al., 2012). To solve the

problem of over-segmentation and sensitivity to noise in traditional watershed algorithm, Zhao et al., 2008 proposed a new method for this. Watershed algorithm was combined with the opening-closing operations and distance transform which overcame all the disadvantages of classical watershed algorithm (Zhao et al., 2008).

SOBEL EDGE DETECTOR

Kaganami & Beiji, 2009 reviewed the main approaches of partitioning an image into regions by using grey values in order to reach a correct interpretation of the image. It compared the region-based segmentation with the boundary estimation using edge detection. The region- segmentation in spite of improving multi-spectral images has the drawback of being applied only on closed boundaries. It used the technique of performance metrics and Canny edge detection. Canny, was able to find pixels near edges but is less able to find exact edges (Kaganami and Beiji, 2009). A new framework to improve the performance of Sobel operator was proposed by Zhang et al., 2012. A method called Sobel operator 2-D maximum entropy segmentation was proposed. First of all segmentation is carried out. Then, segmentation is done by 2-D maximum entropy segmentation approach using thresholds from Sobel edge detector. This method was found to be effective and robust (Zhang et al., 2012). A work by Gao et al., 2010 was proposed which focused on improving Sobel edge detection. The work was carried out on the images with white Gaussian noise. Initially, noise was removed using soft-wavelet threshold method. This method was found to be more effective than the traditional Sobel edge detector (Gao et al., 2010). Sobel method was extended for the improvements in detection. Image was smoothened using Gaussian smoothing. Sobel method was applied to the smoothened image. Fine-to-coarse tracking technique was used for combining the results. This method was superior to the traditional Sobel edge detector. This prevents the edge displacements. But it has a disadvantage of high complexity (Lopez-Molina et al., 2011).

2.5.2. SUPPORT-VECTOR MACHINE TECHNIQUE

As SVM algorithm is time consuming, hence it is combined with distance classifier for texture image classification purpose. The combined technique is called as ISD i.e. integrated SVM and distance classification. A rejecting rule is defined. Distance classifier classifies the image or rejects the image. The rejected image is given to SVM for classification. This technique has low error rate when compared to single SVM (Ma et al., 2002). A classification approach for hyperspectral data using SVM was conducted by Dai et al., 2007. It was compared with traditional classification algorithms. It was found that SVM was more accurate than other algorithms and had ability to handle complex problems (Dai et al., 2007). A study was conducted by Men et al., 2009 which used neural network and support vector machine for classification purpose. In support vector machine two types of kernel functions are used i.e. polynomial and radial basis function. A penalty factor C was also used for improving the classification accuracy. The results indicated that support vector machine was superior to neural network algorithm with more than 96% accuracy (Men et al., 2009). Modified SVM was presented in a study conducted by Zhuo & Lili, 2010. Traditional SVM is quite slow when dealing with the large training sets. This may affect the classification accuracy. The modified SVM is called as RS-SVM i.e. rough set and support vector machine. This improves the accuracy and computational time (Zhuo and Lili, 2010). The pixel-based and object-based classification techniques were compared to each other. The experiment was performed on Landsat-7 ETM+. Support vector machine was utilized for the classification purpose. Statistical analysis was used for accuracy assessment. Statistical parameters used in this paper were overall accuracy, kappa coefficient, Z-score, F-coefficient and ROC curves. All these measures

suggested that object-based segmentation is more appropriate than pixel-based techniques (Zerrouki and Bouchaffra, 2014). The comparative analysis was made between pixel-based classification approach and object-based classification approach in arid environment. The study was conducted on high spatial resolution imagery of 2.5m. Vegetation index and image texture was used for classification. Algorithm used for the classification was support vector machine (Zhang and Jia, 2014). The comparison of the pixel-based and object-based approaches was made in urban environment. The study was conducted on WorldView-2 using support vector machine algorithm. Two cases were considered. First one used training and testing pixels in same reference, whereas second one considered training and testing in separate reference. The object-based technique was found to be useful for former case and pixel-based approach was useful for latter case (Wu et al., 2014).

3.   MATHEMATICAL CONCEPTS OF ALGORTIHMS USED

This chapter deals with the mathematical concepts related to all the techniques used in this research work. This also details the classification techniques for both pixel-based and object-based approach.

3.1.   PIXEL-BASED CLASSIFICATION APPROACH

The mathematical concepts related to pixel-based classification approach are shown in the sections below. There exists eight algorithm which were implemented for this study.

3.1.1.   CONSTRAINED ENERGY MINIMISATION (CEM)

Constrained Energy Minimization (CEM) uses a finite impulse response (FIR) filter to restrain the desired signature by a specific gain at the same time as minimizing the filter output power. It can be derived as (Chang et al., 2015) (Ren et al., 2003) follows. Suppose finite set of observations are represented by S as shown in equation (3.1).

$$S = \{r_1, r_2, \ldots \ldots r_n\} \tag{3.1}$$

Input image pixel vector is represented as, p in equation (3.2).

$$p = \{p_{i1}, p_{i2}, \ldots \ldots p_{iL}\}^T \tag{3.2}$$

Where, $1 < i < N$

N = Total number of pixels in the input image.

L = Total number spectral bands in the input image.

The objective of the algorithm is to detect the targets in the input imagery. Hence, desired targets are represented by d as shown in equation (3.3).

$$d = \{d_1, d_2, \ldots \ldots d_L\}^T \tag{3.3}$$

The CEM algorithm finds the desired target from the imagery using FIR i.e. finite impulse response filter. Hence, assume that there are L coefficients of the filter denoted by w as shown in equation (3.4).

$$w = \{w_1, w_2, \ldots \ldots w_L\}^T \tag{3.4}$$

Output of the FIR filter is denoted by y_i as in equation (3.5).

$$y_i = \sum_{l=1}^{L} w_l r_{il} = w^T r_i = r_i^T w \tag{3.5}$$

Average output power is given in equation (3.6)

$$\frac{1}{N}\left[\sum_{i=1}^{N} y_i^2\right] = \frac{1}{N}\left[\sum_{l=1}^{L} (p_i^t w)^T p_i^T w\right] = w^T\left(\frac{1}{N}\left[\sum_{i=1}^{N} p_i p_i^T\right]\right)w = w^T P_{L\times L} w \tag{3. 6}$$

FIR filter tends to minimize the output subjected to the constrained as in equation (3.7).

$$d^T w = \sum_{l=1}^{L} d_l w_l = 1 \tag{3. 7}$$

$$\text{Where, } P_{L\times L} = \frac{1}{N}\sum_{l=1}^{N} p_l p_i^T = 1 \tag{3. 8}$$

Hence, the operator with weight in equation (3.9) will be:

$$w^{CEM} = \frac{P^{-1}}{d^T P^{-1} d} \tag{3. 9}$$

3.1.2. MATCHED FILTER (MF)

The matched filter (MF) is a traditional method of target detection for multispectral and hyperspectral image. Let the input spectral signal from input L band multispectral/hyperspectral image be x as shown in equation (3.10) (Kwon and Nasrabadi, 2007) (Gao et al., 2009) (Manolakis et al., 2007).

$$x = \{x_1, x_2, \dots . x_L\}^T \tag{3.10}$$

Each input vector can be modeled as desired signal and noise signal as in equation (3.11).

$$x = as + n \tag{3.11}$$

Where, a = attenuation constant (target abundance measure)

$$\text{When, } \begin{cases} a = 0, & \text{Target Absent} \\ a > 0, & \text{Target present} \end{cases}$$

The optimum linear matched is designed in such a way that the desired target signal s is passed through while the output signal-to-noise ratio is maximized, as shown in equation (3.12).

$$\text{Filtered Output, } Y = w^T x = w^T s + w^T n \tag{3.12}$$

On solving the equations in the same way as constrained energy minimization operator, w was calculated as in equation (3.13).

$$w = \frac{C^{-1} s}{s^T C^{-1} s} \tag{3.13}$$

Where, C = covariance matrix of noise

This is classical matched filter. Correlation matrix should be find out for mean-subtracted data. If filtered output is greater than threshold the target is present but if it is less than threshold then target is absent. For non-Gaussian noise matched filter is not optimal. Matched filter maximizes the SNR i.e. signal to noise ratio at the output of an FIR (also IIR) filter (even if the noise is non-Gaussian).

3.1.3. ORTHOGONAL SUBSPACE PROJECTION (OSP)

Orthogonal subspace projection (OSP) is a useful technique in hyperspectral image detection. It estimates the abundance of a target in each pixel. Detection is achieved using a thresholding process. The input signature matrix S is divided into two parts, desired signature of interest d and undesired signature matrix U (Du et al., 2002). 'd' is the first endmember signature s1, and 'U' is the undesired signature matrix [$s_2 \ldots s_p$] i.e. S = [s U] (Du et al., 2003). Input pixels of hyperspectral image is given by equation (3.14).

$$r = da_d + Ua_U + n \qquad (3.14)$$

Where, a_d = Scalar quantity showing abundance of desired pixels.

a_U = Scalar quantity showing abundance of undesired pixels.

OSP classifier projector is as shown in equation (3.15).

$$P_{OSP} = P_U^\perp \qquad (3.15)$$

Where, $P_U^\perp$ = orthogonal complement projector that maps the data onto a subspace orthogonal to undesired signature U. Other form is presented as in equation (3.16).

$$P_{OSP} = \left(d^T P_U^\perp d\right)^{-1} P_U^\perp d \qquad (3.16)$$

This algorithm works well in an environment having known image scene.

3.1.4. ADAPTIVE COHERENCE/COSINE ESTIMATOR (ACE)

The adaptive coherence/cosine estimator (ACE) is hypothesis-test-based detection algorithm. It formulates the target detection as binary hypothesis test problems and then use the likelihood ratio (LR) test and the generalized LR test to obtain the detectors. In this first data whitening is performed (Yang and Shi, 2014) (Shi et al., 2013). Output of ACE detector is given in equation (3.17).

$$y_{ACE}(x) = \frac{\left(x_0^T C^{-1} d_0\right)^2}{x_0^T C^{-1} x_0 d_0^T C^{-1} d_0} \qquad (3.17)$$

Where, C^{-1} = Estimated covariance matrix.

x_0 = Mean-removed input pixel vector.

d_0 = Mean-removed desired pixel vector.

After whitening transform equation reduces to (3.18).

$$y_{ACE}(x) = \frac{(x^T d)^2}{\| x \|^2 \| d \|^2} = \cos^2\theta \tag{3.18}$$

Where, θ = Spectral angle between a and d.

3.1.5. TARGET-CONSTRAINED INTERFERENCE MINIMISATION FILTER (TCIMF)

Target-Constrained Interference-Minimized Filter (TCIMF) assumes that an input image pixel is made up of three separate signal sources (Wang et al., 2013), i.e. D (desired targets), U (undesired targets) and I (interference). It is shown mathematically as under (Ren and Chang, 2000) :

Desired target vector is given in equation (3.19).

$$d = \{d_1, d_2, \ldots \ldots d_L\}^T \tag{3.19}$$

Undesired target vector is given in equation (3.20).

$$U = \{u_1, u_2, \ldots \ldots u_L\}^T \tag{3.20}$$

It also works in a similar manner as CEM. But filters' output is subjected to constraint as given in equation (3.21).

$$[D \ U]^T w = \begin{bmatrix} 1_{p\times1}^T & 0_{q\times1}^T \end{bmatrix}^T \tag{3.21}$$

Where, $1_{p\times1}^T$ = Column vector with one in all components.

$0_{q\times1}^T$ = Column vector with zeros in all components.

Hence, optimal weight comes out to be as shown in equation (3.22).

$$[w]^{TCIMF} = R_{L\times L}^{-1}[D \ U]\left([D \ U]^T R_{L\times L}^{-1}[D \ U]\right)^{-1}\begin{bmatrix} 1_{p\times1}^T & 0_{q\times1}^T \end{bmatrix}^T \tag{3.22}$$

It improves the CEM removing its anomaly of ignoring the information about undesired targets.

3.1.6. MIXTURE TUNED TARGET-CONSTRAINED INTERFERENCE MINIMISATION FILTER (MTTCIMF)

This algorithm is a combination of MTMF (mixture tuned matched filtering) and TCIMF (target-constrained interference minimization filter) algorithms. The only difference between TCIMF and MTTCIMF is that, the latter adds an infeasibility image to the results. The addition of infeasibility image helps in reducing the false positives. MNF transformed image is used as input to the MTTCIMF. While, the output of MTTCIMF is a set of images corresponding to TCIMF score and a set of images including the infeasibility value for each pixel. The TCIMF score estimates degree of match to the reference

spectrum and the approximate sub-pixel abundance, where 1.0 is a perfect match. The infeasibility results are in noise sigma units and indicate the feasibility of the TCIMF result. Correctly mapped pixels have a high TCIMF score and a low infeasibility value. If non-target information is available, MTTCIMF has great potential to reduce the number of false positives over MTMF (Jin et al., 2009).

3.1.7. MIXTURE TUNED MATCHED FILTERING (MTMF)

MTMF follows an additive model in which target pixels actually replaces the background pixel values. This is better than matched filter as it combines both matched filter and spectral unmixing methods. It is useful in case of sub-pixels and has very low false alarm rates. MTMF follows three steps; (1) MNF transformation which is a conditioning step. This includes whitening of the data and mean subtraction as well. (2) Matched filtering is performed for the transformed data. This helps in estimation of target and background abundance. (3) Mixture tuning is done for the output of the matched filter. Infeasibilities are also calculated in this step to reduce the false positive (Boardman and Kruse, 2011).

3.1.8. SPECTRAL ANGLE MAPPER (SAM)

SAM i.e. spectral angle mapper is an easy method for target detection which has existed for a long time. It finds the spectral similarity between the test pixels and the reference spectrum. This algorithm is simple but its disadvantage is that it is sensitive to noise due to which it may cause wrong match. It calculates the angle between the test pixel and reference (or training pixels) (Racek and Baláž, 2012). Assume each spectrum as a vector as shown in equation (3.23).

$$x = (\{x_1, x_2, \dots \dots x_L\}) \tag{3.23}$$

Where, L = number of spectral bands.

The head of the vector is a point in n-dimensional space with the radiance values. Illuminance affects the length of the vector, not its orientation. Whereas, the orientation of the vector is function of the shape of spectral curve. Consequently the orientation (angle) of the vector can be utilized as a robust tool for evaluating similarity between two spectral curves.
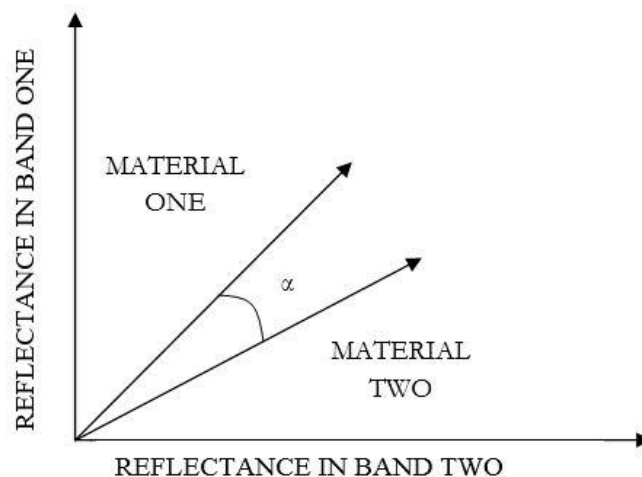

Figure 3-1 Spectral angle mapper concept

Angle between two vectors is given by equation (3.24) and shown in figure (3-1).

$$\alpha = \cos \frac{\sum_{i=1}^{n} x_i y_i}{\sqrt{\sum_{i=1}^{n} x_i^2} \sqrt{\sum_{i=1}^{n} y_i^2}}$$

(3.24)

Therefore SAM can be reliably utilized for the detection of pure spectra.

3.2. OBJECT-BASED CLASSIFICATION APPROACH

The mathematical concepts related to object-based classification approach are shown in the sections below. There exists eight algorithm which were implemented for this study.

3.2.1. SUPPORT VECTOR MACHINE

This section describes support vector machine algorithm i.e. SVM for image classification problems. Support vector machine is a particular class of algorithms, portrayed by the use of kernels. We consider here a case of two class classification problem. The support vector machine algorithm is a new technique which uses a function in such a way that the function is able to differentiate between two sets of training data minimizing the error. It is a bit slow when dealing with large quantity of data. This in turn affects the classification accuracy. It is based on optimization technology (Zhuo and Lili, 2010). The simplest form of SVM is two-class classification which helps in deciding whether a training pixel belongs to a class or not. Two types of training sets i.e. positive and negative pixels are given to SVM algorithm. All the pixels are converted to n-dimensional vector. It finds a hyper-plane to separate positive and negative pixels. Consider training data as vector of pixel values and class label as mentioned in equation 3.25 (Zhang et al., 2001):

$$\{(x_1, c_1), (x_2 c_2), \dots, (x_k y_k)\}$$

(3.25)

Where, x_i = input image vector with k bands.

c_i = +1, -1 binary decision function for class labelling.

These pixel values can be separated into two classes using a hyperplane as shown in figure 3-2. SVM classifier can also be used as non-linear classifier by using non-linear kernel.
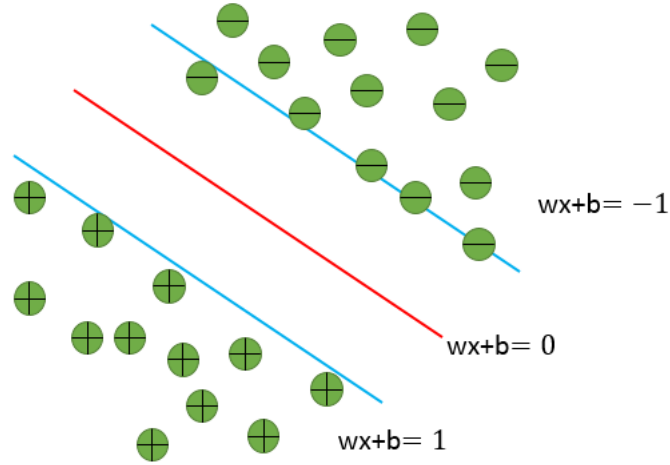
Figure 3-2 Hyper plane

Let the weight and the bias of the separating hyper plane is w and b, respectively. Where w is the adjustable weight vector, x is the input vector and b is the bias. We define a hyper plane which might act as decision surface in feature space, as given in equation (3.26).

$$\sum_{j=1}^{l} w_j \emptyset_j (x) + b = 0$$

(3.26)

For the maximum separation of the two training sets, the distance of this hyper- plane to the nearest data points should be maximized. Two parallel hyper-planes can form the hyper-plane with maximum margin. These margins (i.e. the two parallel hyper-planes) should pass at least one vector (data point) of the two classes. These vectors are called support vectors and are indeed, the nearest data points to the hyper-plane. Other training data have no influence in definition of the separating hyper-plane and therefore, have no influence in classification algorithm.

The nonlinear SVM is used when the data points cannot be separated by a simple straight line. Thus, a kernel function has to be used to solve this problem. With a kernel function, the data points are transformed into feature space so that the data points can be separated, and the optimal separating hyperplane can be achieved. The decision function implemented in that space can be written as equation (3.27):

$$f(x) = sgn\left(\sum_{j=1}^{N} y_j a_j k_j (x_i, x_j) + b\right)$$

(3.27)

Where, b is the bias, a_j is the weight vector, y_j is the target vector, $k_j(x_i, x_j)$ is the inner product kernel and N is number of support vector. The quality of the SVM models depends on the kernel type and

various parameters that control the kernel shape. There are four typical kernel functions; linear, polynomial, quadratic and RBF.

Linear kernel:

A linear SVM (LSVM) is based on determining an optimum hyperplane that separates the data into two classes with the maximum margin. The LSVM typically has high classification accuracy for linearly separable data. However, for nonlinearly separable data, LSVM has poor performance. For this type of data, a nonlinear SVM (NSVM) is preferred. The NSVM transforms the input data using a nonlinear kernel followed by the LSVM. Although the NSVM can achieve higher classification performance, it requires high computation time to map the input to a higher dimensional space by a nonlinear kernel function which is usually a fully dense matrix.

Linear kernel is known as the dot product. It is the most efficient kernel which produces output values by combining all support vectors linearly, as shown in the following equation (3.28).

$$k_j(x_i, x_j) = x_i . x_j \qquad (3.28)$$

4. STUDY AREA AND DATASET USED

This chapter describes the study area and satellite/airborne data utilized for the study. The section 4.1 provides the description of two study areas corresponding to two datasets used. The second section 4.2 describes the two datasets used i.e. airborne LWIR hyperspectral data and ASTER thermal data to aid the processing.

4.1. STUDY AREA

This research work was carried out for following two different study areas:

1. Study Area 1: Black lake area of Thetford Mines in Quebec, Canada.
2. Study Area 2: Dehradun in Uttarakhand, India.

4.1.1. STUDY AREA 1

The study area 1 corresponding to airborne LWIR hyperspectral data is located in black lake area of Thetford Mines, in province of Québec, Canada. Thetford Mines is a town in south-central Quebec which is rich in serpentine rocks. The latitude and longitude of this area is 46.047927°N and 71.366893°W respectively. The region is a mosaic of various natural and man-made objects. The material for constructing the road is asphalt and for the sidewalks concrete is used. Roofs are built using asphalt shingles whereas flat roofs are protected with the covering of elastomeric membrane. The roofs of garages and sheds are fabricated with the help of sheet metal ("The 2014 IEEE GRSS Data Fusion contest: description of the datasets," 2014). The Google earth imagery of the first study area is as shown in figure: 4-1.

Figure 4-1 Google earth image showing the study
area 1

4.1.2. STUDY AREA 2

The other study area (Study area 2) used corresponding to multispectral thermal data (ASTER data) covers Dehradun and its surroundings in Uttrakhand state of India. Dehradun city is the capital of Uttrakhand state. The city is one of the ancient cities of India. Dehradun city of Uttrakhand in India covers an area of 300 square km. Its central latitude is 30.442946°N and central longitude is 78.225994°E. It is a main tourist spot of India (Nand and Kumar, 1989). It is shown in figure 4-2.
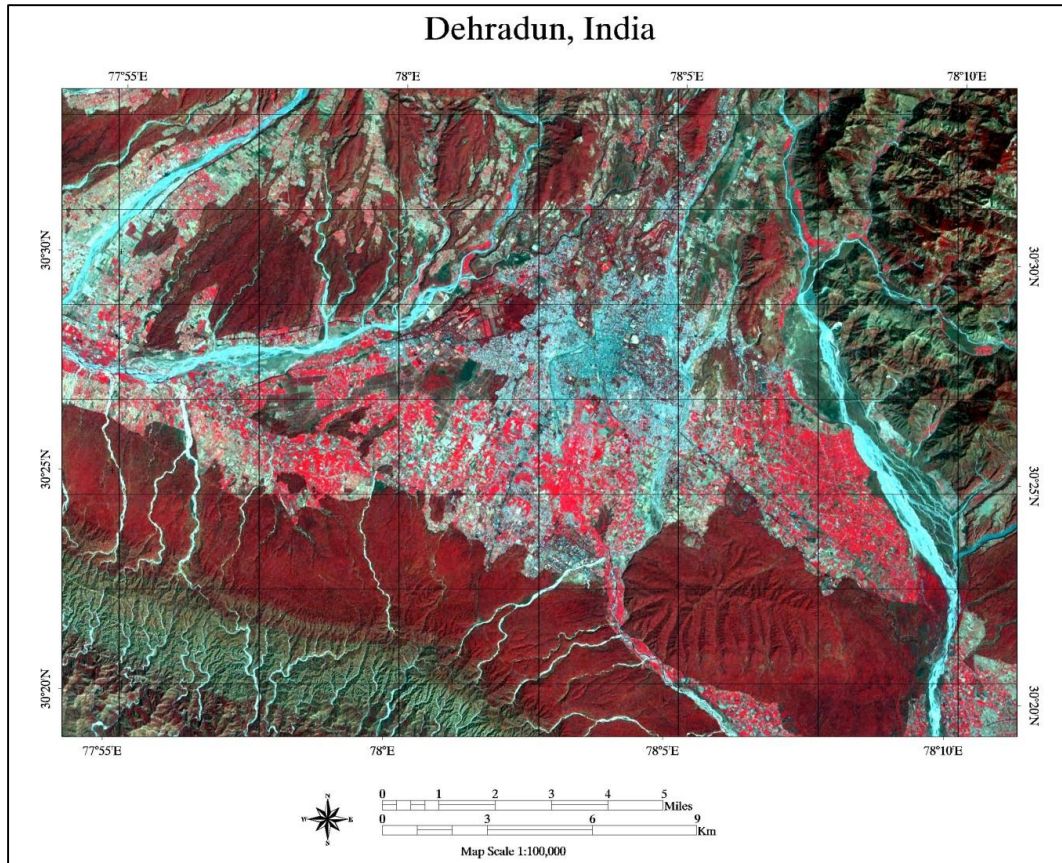

Figure 4-2 ASTER image displaying the study area Dehradun, India

4.2. DATASET'S DESCRIPTION
4.2.1. DATASET USED 1

The following datasets have been used corresponding to study area 1 (Quebec, Canada) and the details have been shown in table ("The 2014 IEEE GRSS Data Fusion contest: description of the datasets," 2014) 4-1.

1. Airborne LWIR (long wave infrared) hyperspectral dataset of the city.
2. High resolution coloured digital photograph of the same area, with sparse ground coverage.
3. Ground truth image.

Table 4-1 Hyperspectral dataset description

Dataset #	Dataset Type	Features
1	Airborne LWIR hyperspectral image	Georeferenced, 751×874 pixels, Bands: 84, BSQ, 32 bits per pixel and channel.
2	Coloured digital photograph	Georeferenced , RGB uncalibrated data, 3769×4386 pixels, BSQ, Unsigned integer format with 8 bits per pixel.
3	Ground truth image	Showing locations of various classes with legend.

1. **Airborne LWIR Hyperspectral Dataset**: The airborne dataset was acquired by Telops over low density area. The sensor used to acquire the first dataset i.e. airborne LWIR hyperspectral imagery was acquired by Telop's Hypercam sensor which is an airborne long wave infrared hyperspectral imager. This imager is based upon Fourier Transform spectrometer (FTS). It was mounted on a gyro-stabilized platform in an aircraft. The number of bands in LWIR imagery are 84 bands in 868 cm^{-1} 1280 cm^{-1} region (7.8 μm to 11.5 μm). Its spectral resolution is 6 cm^{-1} (full-width-half-maximum) and average spatial resolution (GSD) is 1m. This data is in the form of "at-sensor spectral radiance" in W/(m^2 sr cm^{-1}). The imagery is presented in figure 4-3.
2. **Coloured digital photograph:** This dataset was captured with the help of a coloured digital camera of 2 megapixels, also mounted on the same gyro-stabilized platform in the aircraft. This covers the same ground area as covered by LWIR imagery. The spatial resolution of the coloured digital photograph is 0.2 m. Figure 4-3 represents the second dataset i.e. coloured digital photograph. Both the airborne datasets were georeferenced and mutually registered. The average height for both the sensors is 2650 ft (807m) and were acquired concurrently on May 21, 2013, between time 22:27:36 to 23:46:01 UTC.
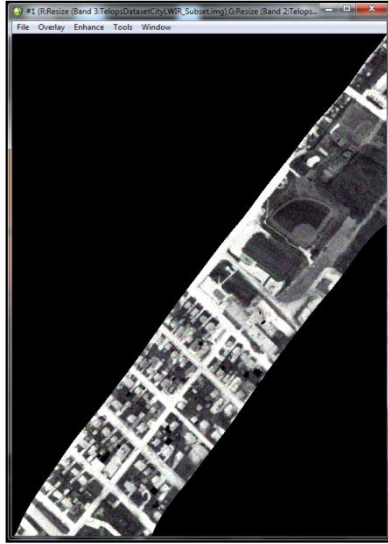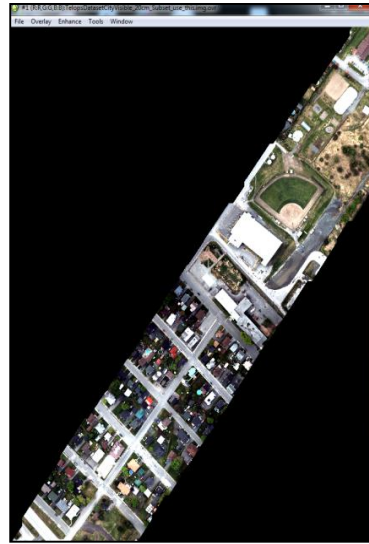
Figure 4-3 Airborne LWIR hyperspectral dataset   Figure 4-4 Coloured Digital Photograph

3. **Ground Truth image:** The ground truth image was also provided along with LWIR dataset showing the locations of all the seven classes i.e. road, vegetation, tree, bare soil, red roof, concrete roof and grey roof. From this ground truth dataset some of the pixel samples were considered as training pixels and rest of them as testing pixels. Ground truth data has been shown in figure 4-5 with the corresponding legend.
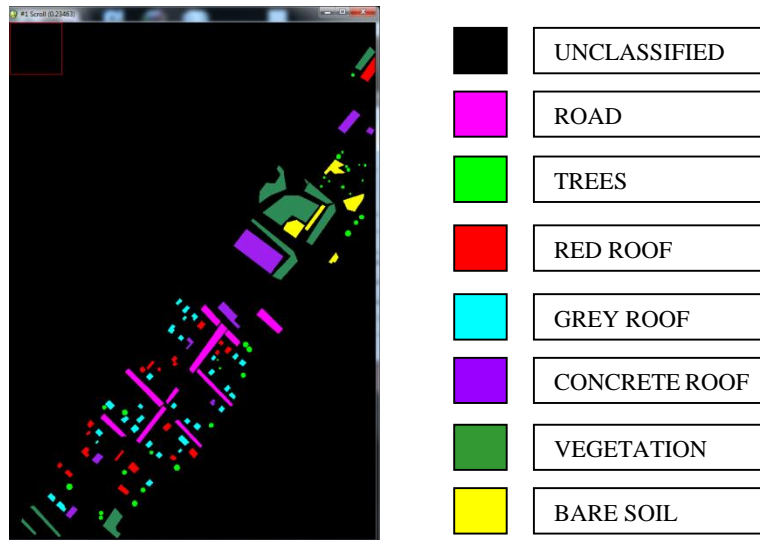

Figure 4-5 Ground truth location and Legend

4.2.2. DATASET USED 2

ASTER i.e. Advanced Spaceborne Thermal Emission and Reflection Radiometer is a sensor on Terra satellite launched in December 1999. It has 14 bands covering visible to infrared region. The spatial resolution is 15m for visible region and near-infrared region, 30m resolution in short-wave infrared region and 90m resolution in thermal infrared region. Visible region has 3 bands, SWIR has 6 bands and

TIR has 5 bands. Details of 14 bands in the visible and infrared spectrum with different spatial resolutions (VNIR at 15m, at 30m, TIR at 90 m) have been given in Table 4-2 (JPL, 2004).

Table 4-2 Characteristics of the ASTER sensor systems

BAND NAME	BAND NO.	SPECTRAL RANGE (μm)	SPATIAL RESOLUTION (m)	QUANTISATION LEVELS
VNIR	1	0.52-0.60	15	8 BITS
	2	0.63-0.69		
	3N	0.78-0.86		
	3B	0.78-0.86		
SWIR	4	1.60-1.70	30	8 BITS
	5	2.145-2.185		
	6	2.185-2.225		
	7	2.235-2.285		
	8	2.295-2.365		
	9	2.360-2.430		
TIR	10	8.125-8.475	90	12 BITS
	11	8.475-8.825		
	12	8.925-9.275		
	13	10.25-10.95		
	14	10.95-11.65		

5. METHODOLOGY

This section provides an overview of the methodology adopted in this research. The methodology is divided into two parts: pixel-based approach and object-based approach. The pixel-based and object-based classification approach is depicted in figure 5.1 and 5.2. A broad division of the workflow (each segment is explained subsequently) have been illustrated.

IMAGE PRE-PROCESSING:

The airborne LWIR hyperspectral data was made available after pre-processing and atmospheric correction. This dataset was interpreted in terms of classes (or objects) constituted in the study area and identification of crucial training and testing data sites. Besides the high spectral resolution (of 84 bands), the dataset has a fine spatial resolution of 1meter. An attempt was initiated for better identification of specific classes from the airborne hyperspectral data. The objects identified from airborne LWIR hyperspectral data were as follows:

1. Trees
2. Road
3. Vegetation
4. Bare soil
5. Red Roof
6. Concrete Roof
7. Grey Roof

The objects identified from ASTER multispectral data were as follows:

1. Urban area
2. Forest
3. Agriculture area with crop
4. Water
5. Sand

Airborne LWIR hyperspectral image has high spectral and spatial resolution but it is a little noisy which makes it difficult to process it. Some of the bands in the thermal data i.e. band number 80, 81 and 82 were removed as they were very noisy and did not contain much information. Also, the thermal data was resampled to 0.2 m in order to combine it with coloured digital photograph.

DATA DIMENSIONALITY REDUCTION TECHNIQUE:

Airborne LWIR Hyperspectral remote sensing data and combination of airborne LWIR hyperspectral data with coloured digital photograph are of high dimension i.e. with 84 bands and 84 bands + 3 bands (R, G, B). They have high data capacity and have spectral redundancies manifested as high correlations between adjacent bands. The disadvantage of this redundancy is (a) increase in computational complexity; (b) vitiate classification accuracy. So this calls for dimensionality reduction for both these datasets. Dimensionality reduction technique projects high dimension data to lower dimension data

without mislaying information. Some of the techniques for feature extraction are: MNF, PCA and canonical transformations.

This research work uses a traditional dimensionality reduction approach i.e. minimum noise fraction (MNF) to reduce the number of features for the airborne LWIR hyperspectral data and for combination of thermal data with coloured digital photograph. This step reduces the number of bands and diminishes the noise in the datasets. There are two types of data dimensionality reduction approaches that are available in literature i.e. feature selection and, feature extraction. Out of these feature selection approaches do not distort the original data through a transformation, hence is useful for interpretability, transferability over space and time. The other is feature extraction in which after transformation original data is not preserved. Hence, some critical information may be distorted. Compared to the feature extraction, band selection technique has an advantage of preserving original information from the data. On the other hand, it also suffers from two problems. One problem is the number of bands for preserving the information and other is appropriate criterion for the selection.

Two traditional and standard techniques for dimensionality reduction is principal component analysis (PCA) and minimum noise fraction (MNF). Principal Component Analysis (PCA) is most widely used method of compressing the data. It generates new features through linear combinations of the original features, orthogonal to each other. One shortcoming of PCA technique is that it does not always produces image with decreasing image quality with decreasing principal components. So, we chose other approach called minimum noise fraction MNF. This method arranges the image components in order of decreasing image quality. This maximizes the signal-to-noise ratio i.e. SNR.

The airborne LWIR hyperspectral data consists of 84 bands. Hughes phenomenon and training data restricts classification without dimensionality reduction. The MNF components are generated, displaying the respective Eigen values and percentages of information contained in the respective components (Figure 5-1). Figure 5-2 graphically illustrates the reduction in gain of information with increasing MNF components. Depending on the amount of information and lack of gain of variance in the increasing MNF components, the initial intrinsic dimensionality is reduced to 7 components. However, the best possible components or MNF components input database was determined from the results of the classification. The combination of optimal number of MNF components was the considered database used as input for various detection algorithms. Minimum noise fraction (MNF) was applied to both the datasets i.e. airborne LWIR hyperspectral data and combination of LWIR with coloured digital photograph. Then database was created using MNF components from 2 to 7. As the amount of information in MNF graph saturates at value of MNF equal to 7. Each of the MNF component was given as input to target detection algorithms one by one till optimum band number was achieved.
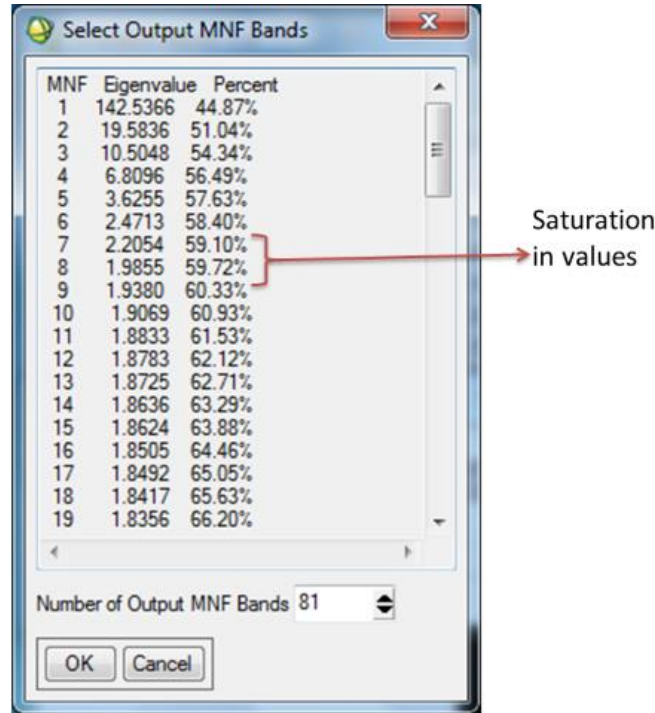
Figure 5-1 Percentage depiction of gain in variance with increase in MNF components
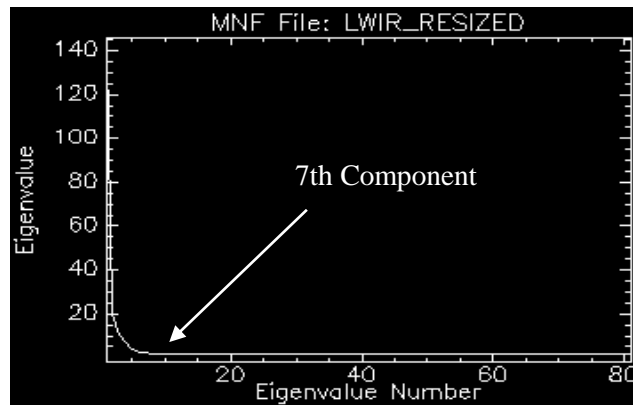

Figure 5-2 Graphical depiction of reduction of variance with increasing MNF components

5.1. PIXEL-BASED CLASSIFICATION APPROACH

The methodology for pixel-based classification approach is shown in figure 5-3. This approach was tested for two types of datasets i.e. airborne LWIR hyperspectral data and combination of thermal data with colored digital photograph. The pixels in ground truth imagery were divided into two sets i.e. training samples and testing samples. Training samples (20 each class) were given as input to pixel-based algorithms. Eight pixel-based higher-order algorithms were used namely, constrained energy minimization (CEM), matched filter (MF),spectral angle mapper (SAM), adaptive coherence estimator (ACE), orthogonal subspace projection (OSP), mixture-tuned matched filter (MTMF), target-constrained interference-minimized filter (TCIMF) and mixture-tuned target-constrained interference minimized filter (MTTCIMF). These algorithms produces grey scale images of the target/object to be detected. For each algorithm, seven grey scale images were generated corresponding to each object i.e.

tree, road, vegetation, bare soil, red roof, concrete roof and grey roof. These grey scale images were combined into one to produce a land-cover map i.e. grey scale images were defuzzified. These defuzzified outputs were used for accuracy assessment for final outputs. Stratified random sampling was used for the generation of points for accuracy assessment. Twenty points per class were generated using stratified random sampling approach. Then, error matrix was generated to find user accuracy, producer accuracy and overall accuracy. The ability of each detector to extract the seven classes were found and judged by comparing user accuracy for each class. Another measure of accuracy of classification used in this paper is overall accuracy which is used to find out best pixel-based algorithm for these datasets. The methodology has been shown in figure 5-3.
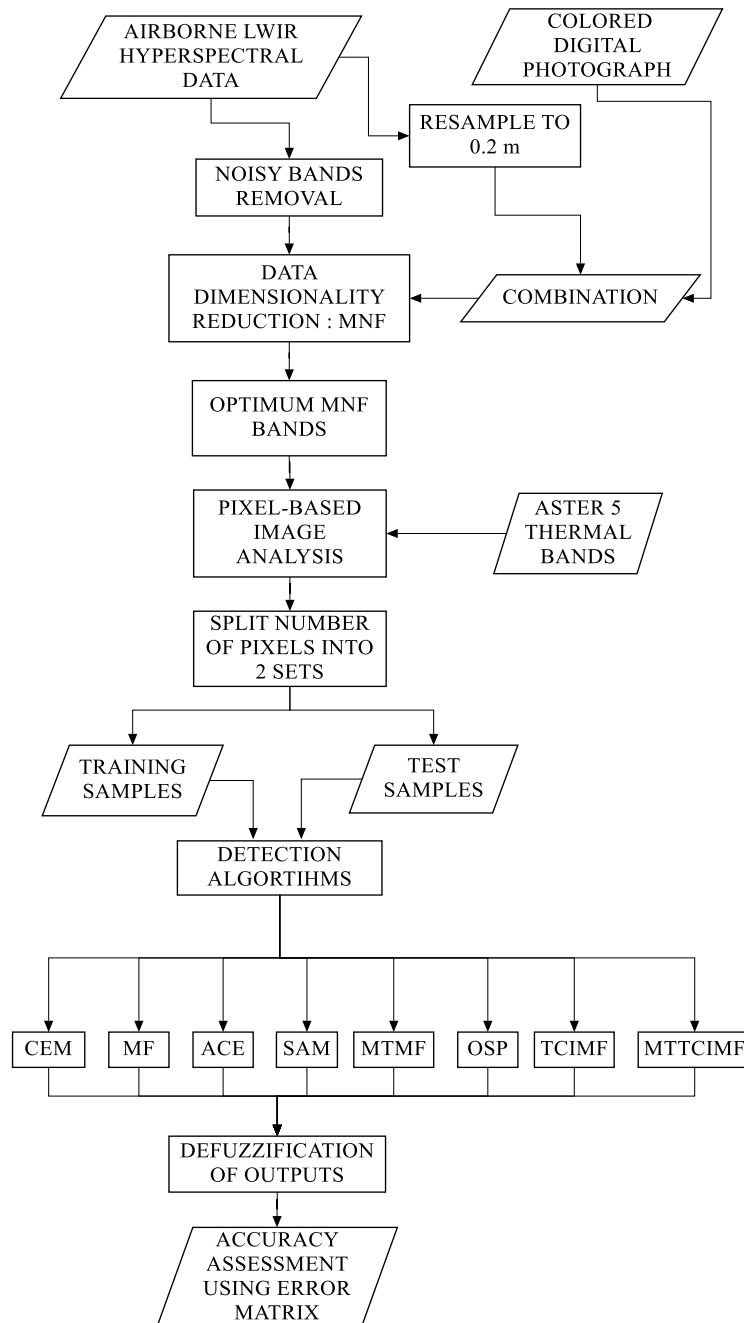

Figure 5-3 Adopted Methodology for Pixel-based approach

5.2. OBJECT-BASED CLASSIFICATION APPROACH

Other approach applied was object-based classification approach. The methodology for object-oriented classification technique is shown in figure 5-4. It consists of two parts: image segmentation, and object classification.
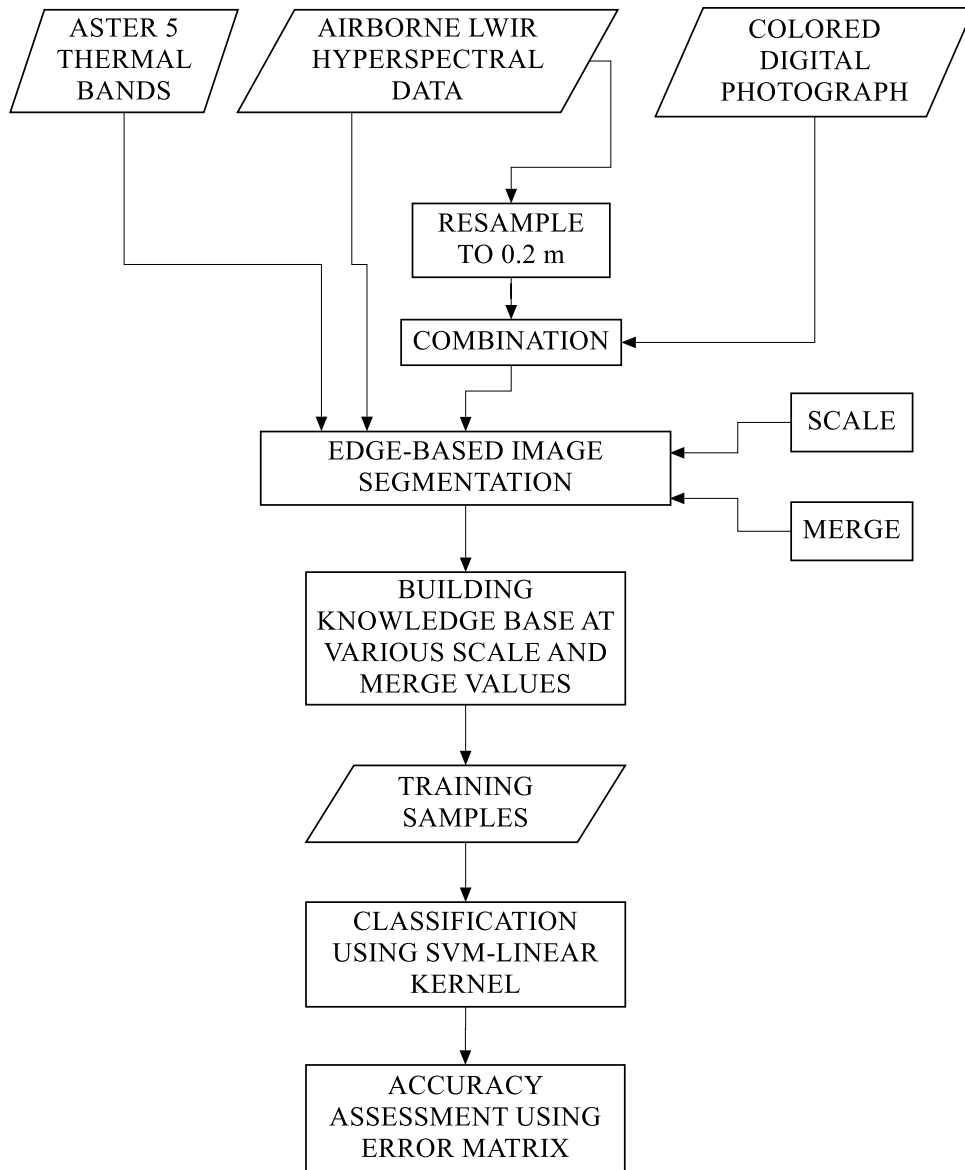

Figure 5-4 Adopted Methodology for Object-based approach

5.2.1. OBJECT SEGMENTATION

Objects are group of pixels. Segmentation process involves grouping of pixels into meaningful objects. The algorithm used in this paper is Sobel edge detector. This algorithm identifies feature with distinct boundaries. In this the highest pixel values are the areas which has highest pixel contrast. Then, the watershed algorithm is applied to the produced gradient image. Segmentation process affects the further classification (Xin et al., 2011). Under-segmentation and over-segmentation process may lead to poor

classification. The main problem in the segmentation procedure is spectral similarity of various features like, similarity of various roof material. Hence, merging of objects is performed.

5.2.2. CLASSIFICATION

The next step is classification. The classification algorithm used in this paper is support vector machine (SVM) with linear kernel (Zhu et al., 2011). SVM is a machine learning algorithm which is quite complex and is very slow. SVM maps the input vector into high dimensional plane through non-linear mapping (Ji et al., 2006). Hence, it classifies data in high dimension. First of all training objects are selected for each class and given as input to classifier. This algorithm finds an optimal hyperplane which can separate various classes. Classification is performed according to the decision function (Rafiee and Saradjian, 2008). In this paper, SVM using linear kernel was implemented. Consider the input image as vector of pixel values with n bands. These pixels belong to one of the seven classes.

DEFUZZIFICATION AND ACCURACY ASSESSMENT

Defuzzification of the all soft outputs in all the cases was done by a simple maximum value approach. The algorithm reads the membership values along the pixel vector and assigns the class with the maximum membership to the pixel. The combination of 7 soft outputs, each corresponding to its respective class, is ― hardened to a single output, containing classification results that can be evaluated by traditional methods of accuracy assessment (user's accuracy), using a combination of user-defined and randomly generated test sites.

The completion of the classification procedure requires implementation of methods to assess the accuracy of the procedure adopted. Considering the fact that the classification approach remains the same for each of the inputs, the end result would be an interpretation of the influence of the input database for classification. Based on various analysis and review, an approach called Accuracy assessment (as a measure of degree of correctness) is used for assessing the classification outputs. The outputs of the classification process are individual, grey-scale class soft outputs. The successful classification of an object class was assessed by a method of mean difference calculations. The illustration depicts a choice of random pixels in known class locations and calculating the difference. If the difference is significant, it implies that the class is separable after classification. If a certain class has been successfully classified, accuracy assessment was used to quantify their accuracy of identification. Generalizing, the particular class shows a better contrast in the output with reference to other classes.

6. RESULTS

This chapter details the results obtained during the course of the present research and elaborates their possible interpretations. Pixel-based and objects-based image analysis (OBIA) approaches have been performed on two datasets i.e. airborne LWIR hyperspectral data and ASTER thermal bands. The accuracy of the classification results using these two approaches were assessed by creating the error matrix using the same test area as reference data. Comparisons of the results of the accuracy assessment showed that object oriented image analysis attains higher overall accuracy and higher land cover class accuracy (producer's accuracy and user's accuracy) for most of the classified land cover class.

6.1. RESULTS FOR PIXEL-BASED CLASSIFICATION

Pixel based image analysis techniques used here were higher-order target-detection algorithms. These algorithms detects the classes by considering an object as target, while other classes as non-target or background. It gives the output result as a gray-scale values. Three basic steps were followed: training stage, classification stage and accuracy assessment stage. Training samples and testing samples were selected from the reference image. For accuracy assessment, error matrix/confusion matrix was generated.

6.1.1. RESULTS FOR AIRBORNE LWIR HYPERSPECTRAL DATA

First of all the pixel-based approach was tested for thermal bands alone. In order to find out best pixel-based algorithm for extraction of each class, the user's accuracy is compared as shown in table 6-1. The classifiers found to be suitable for extraction of each of the seven class are as follows: For extraction of tree, MTTCIMF was suitable as user accuracy is 83.33%. CEM was found suitable for identification of road and bare soil with user accuracy of 97.62% and 83.33% respectively. For vegetation detection, ACE algorithm was found to be apt with user accuracy of 91.67%. OSP detected red roof with user's accuracy of 52.63%. For concrete roof, 60.00% accuracy was obtained using MF. For grey roof, MTMF was suitable with user's accuracy of 87.50%. MTTCIMF, TCIMF and OSP were unable to detect road, bare soil and grey roof as these classes got mixed up with other classes. ACE could not extract grey roof.

Table 6-1 User's accuracy of each class for thermal data

S.no	Algorithm	Tree	Road	Vegetation	Bare Soil	Red Roof	Concrete Roof	Grey Roof
1.	CEM	45.83%	97.62%	64.71%	83.33%	50.00%	53.85%	50.00%
2.	MF	35.71%	95.24%	73.91%	53.85%	50.00%	60.00%	37.50%
3.	SAM	44.44%	85.71%	81.82%	33.33%	50.00%	50.00%	33.33%
4.	MTMF	33.33%	92.00%	63.16%	55.56%	25.00%	33.33%	87.50%
5.	MTTCIMF	83.33%	-----	66.67%	-----	22.22%	50.00%	-----
6.	OSP	58.33%	-----	50.00%	-----	63.64%	54.55%	-----
7.	ACE	80.00%	72.73%	91.67%	27.27%	18.18%	33.33%	-----
8.	TCIMF	55.56%	------	42.86%	-----	20.20%	-----	-----

----- represents misclassification.

It was found that MNF did not give good results when applied to thermal data as shown in table 6-2. Highest accuracy obtained was 81.71% using SAM without application of MNF as a pre-processing step. The best achieved results are shown in figure 6-1 and 6-2. Figure 6-1 represents result with CEM technique and figure 6-2 shows resulting image using SAM technique.
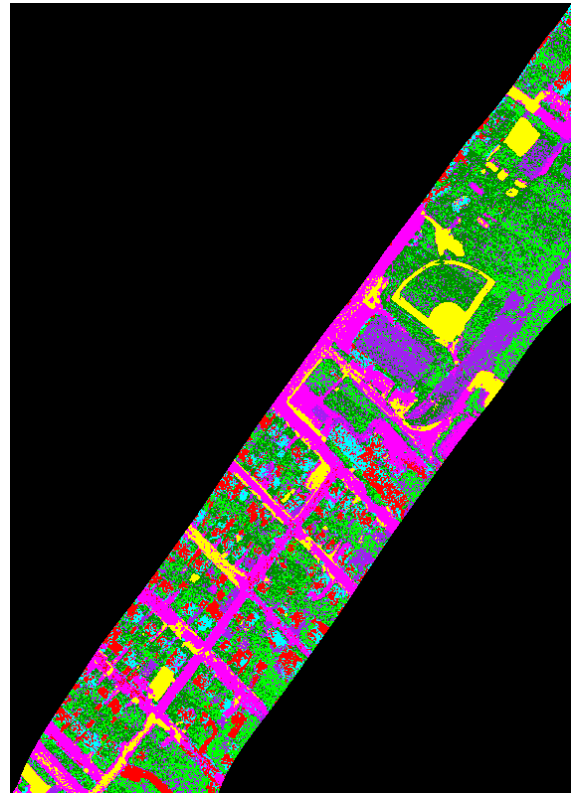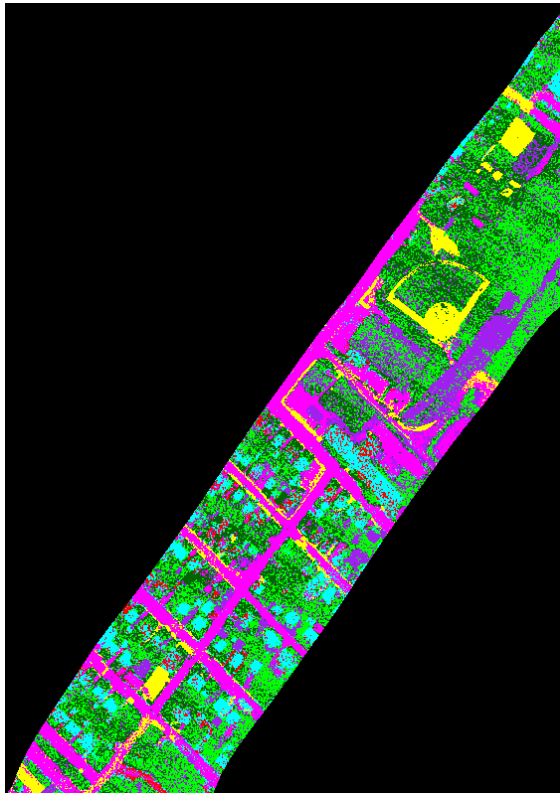

Figure 6-1 Land-cover map for CEM using thermal data

Figure 6-2 Land-cover map for SAM using thermal data

⬛	UNCLASSIFIED
🟪	ROAD
🟩	TREES
🟥	RED ROOF
🟦	GREY ROOF
🟪	CONCRETE ROOF
🟩	VEGETATION
🟨	BARE SOIL

Figure 6-3 Legend

Table 6-2 Comparison of overall accuracy for airborne LWIR hyperspectral data with MNF and without MNF

S.NO	TARGET DETECTOR	OVERALL ACCURACY FOR RESULTS WITH MNF	OVERALL ACCURACY FOR RESULTS WITHOUT MNF
1.	**CEM**	**69.92%**	66.67%
2.	**ACE**	53.57%	57.14%
3.	**MF**	65.12%	65.96%
4.	**OSP**	42.03%	53.29%
5.	**TCIMF**	40.00%	45.09%
6.	**SAM**	63.27%	**81.71%**

6.1.2. RESULTS FOR THE COMBINATION OF AIRBORNE LWIR HYPERSPECTRAL DATA WITH COLOURED DIGITAL PHOTOGRAPH

The same procedure was followed for the combination of thermal data with incorporation of coloured digital photograph. The comparison of user accuracy has been shown in table 6-3. The classifiers suitable for each class are: CEM was found to be suitable for extraction of tree and road with user accuracy of 61.90% and 95.00% respectively. For detection of vegetation and red roof, SAM was suitable with user's accuracy of 92.31% and 77.78%. For bare soil MTMF is suitable as user's accuracy is 80.00%. OSP algorithm was found to be appropriate for detection of concrete roof and grey roof with user's accuracy of 75.00% and 57.14%. CEM, MF, SAM and MTMF were not useful for grey roof detection. SAM was not found to be appropriate for concrete roof. OSP was unsuitable for road.

Table 6-3 User's accuracy for each class with combination of thermal data with coloured digital photograph

S.no	Algorithm	Tree	Road	Vegetation	Bare soil	Red roof	Concrete roof	Grey roof
1.	**CEM**	61.90%	95.00%	80.95%	54.55%	71.43%	21.05%	-------
2.	**MF**	40.00%	87.50%	68.75%	33.33%	69.23%	17.86%	-------
3.	**SAM**	25.00%	35.71%	92.31%	54.55%	77.78%	------	------
4.	**MTMF**	38.46%	81.82%	85.71%	80.00%	33.33%	70.00%	------
5.	**MTTCIMF**	33.33%	66.67%	57.14%	50.00%	46.67%	66.67%	25.00%
6.	**OSP**	66.67%	------	88.89%	50.00%	28.57%	75.00%	57.14%
7.	**ACE**	75.00%	85.71%	55.56%	50.00%	50.00%	50.00%	------
8.	**TCIMF**	------	------	10.00%	75.00%	23.81%	33.33%	15.38%

It was found that MNF did not give good results when applied to thermal data as shown in table 6-4. Highest accuracy obtained was 90.99% using SAM without any MNF as a pre-processing step.
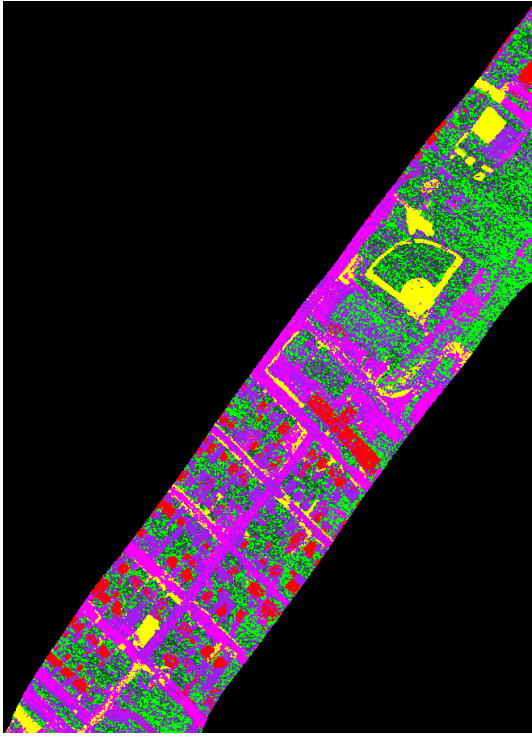
Figure 6-4 Land-cover map for ACE using combination of thermal data with coloured-digital photograph
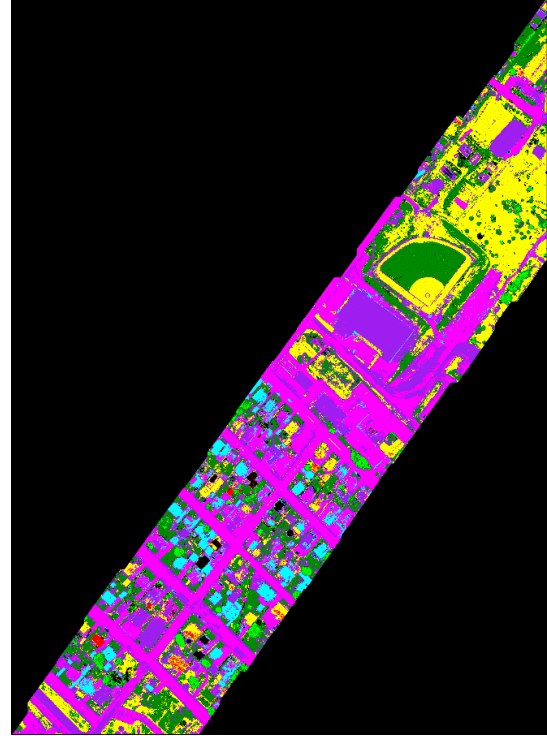

Figure 6-5 Land-cover map for SAM using combination of thermal data with coloured-digital photograph

Figure 6-3 shows resulting image with ACE algorithm with MNF as a pre-processing step and figure 6-4 shows image with SAM without any MNF.

Table 6-4   Comparison of overall accuracy for combination of airborne LWIR hyperspectral data and colored digital photograph with MNF and without MNF

S.NO	TARGET DETECTOR	OVERALL ACCURACY FOR RESULTS WITH MNF	OVERALL ACCURACY FOR RESULTS WITHOUT MNF
1.	CEM	64.65%	73.91%
2.	ACE	66.67%	63.95%
3.	MF	51.85%	77.78%
4.	TCIMF	21.13%	50.96%
5.	SAM	60.78%	90.99%

6.1.3. RESULTS FOR ASTER THERMAL DATA

The best outcome of pixel-based technique i.e. spectral angle mapper (SAM) algorithm was applied to multispectral thermal data i.e. ASTER thermal bands. The angle of 0.08 radians was used for this data which was fined tuned using hyperspectral thermal data. The output image is shown in figure 6-5. The legend is given in table 6-5. The accuracy assessment was performed for this data using error matrix. The overall accuracy came out to be 74.4035% and kappa coefficient of 0.6768. The user's accuracy for each class/object is depicted in table 6-6. From table it was observed that sand and water were classified

with high accuracy of 91.58% and 98.04% respectively. Forest, agriculture and urban area were classified at almost same accuracy level. There was quite misclassification in urban area.
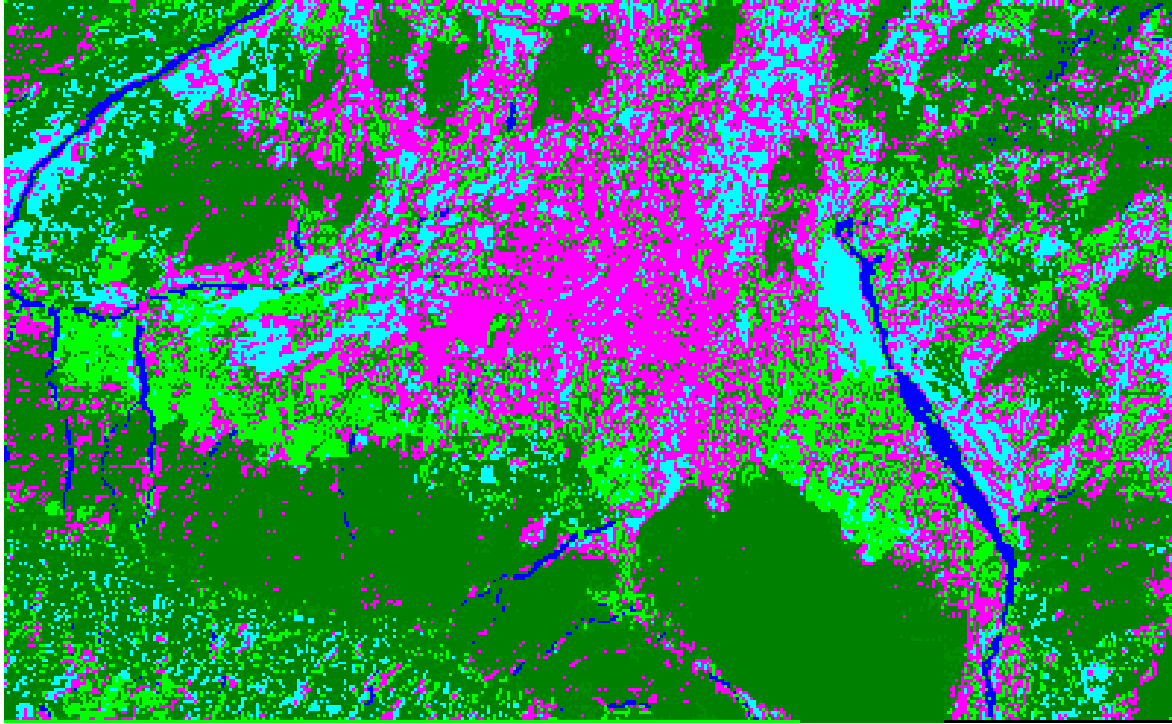
Figure 6-6 Output image for ASTER thermal data using SAM algorithm (0.08 radians)

Table 6-5 Legend

	Forest
	Agriculture
	Urban
	Water
	Sand

Overall Accuracy = 74.4035%

Kappa Coefficient = 0.6768

Table 6-6 User's accuracy for each class using SAM algorithm

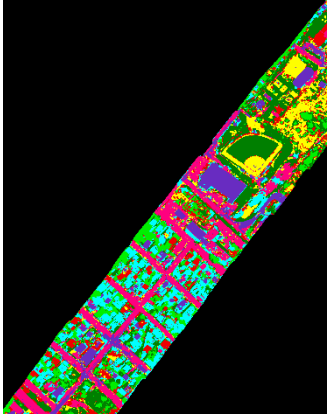| SNO	CLASS	USERS ACCURACY
1	FOREST	64.44%
2	URBAN	65.32%
3	AGRICULTURE	66.34%
4	SAND	91.58%
5	WATER	98.04%
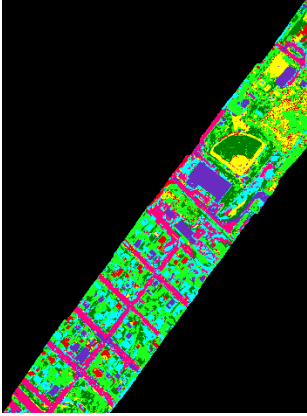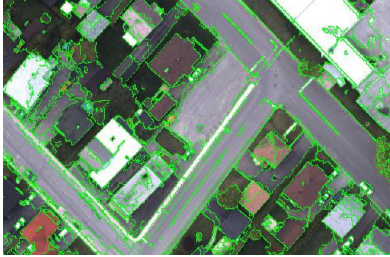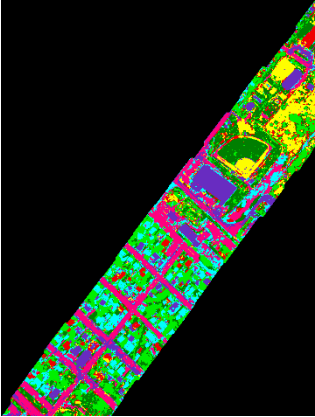
6.2. RESULTS FOR OBJECT-BASED CLASSIFICATION
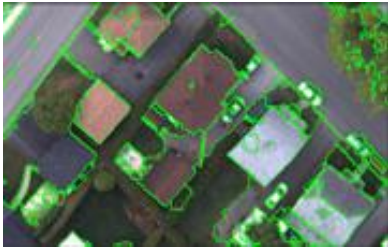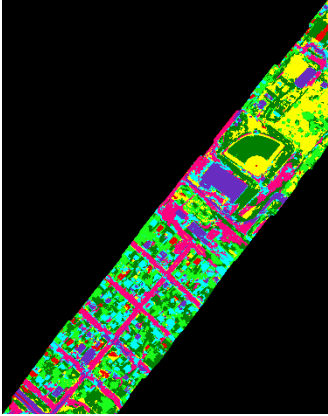
Object-based image analysis techniques used here were constituted watershed algorithm for segmentation and SVM for classification. These algorithms detects the classes first by segmenting the image. Then, it classifies the image using objects as training samples. Three basic steps were followed: segmentation, classification stage and accuracy assessment stage. Training samples and testing samples were selected from the reference image. For accuracy assessment, error matrix/confusion matrix was generated.

6.2.1. RESULTS FOR COLOURED DIGITAL PHOTOGRAPH

Now, the coloured digital photograph (R, G, B bands) is subjected to object-oriented classification technique. The first step in object-based classification is segmentation and merging process. The scale values are chosen in increasing order of 50, 60. 70, and 80. The merge value was set at 90 for all the scale values. The results are compiled in table 6-5.
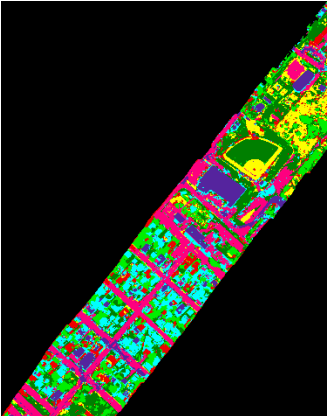
Table 6-7 Overall accuracy for coloured digital photograph from scale values 50 to 80
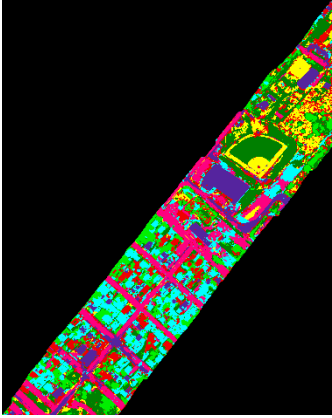
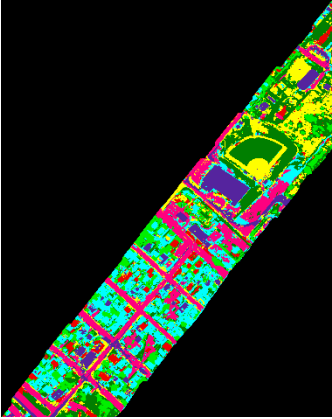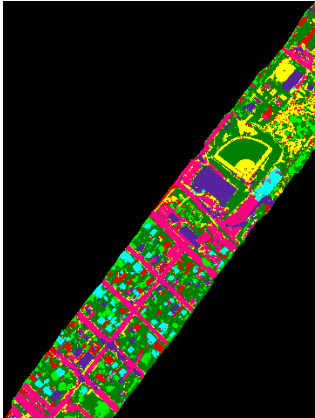| Scale	Merge	Segmented image	Classified image	Overall Accuracy
50	90			60.96%
60	90			65.00%
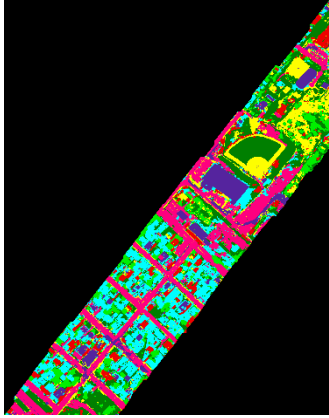
70	90			68.75%
80	90			69.70%

As the overall accuracy was highest at 80, hence scale values were tested from 81 to 85 for fine tuning of overall accuracy. The results are compiled in table 6-6. It is seen from the table that scale value of 83 and merge value of 90 gives highest overall accuracy of 80.00% and kappa value of 0.7638. The value of overall accuracy increases from scale 50 to 83, while 84 onwards it starts decreasing again.

Table 6-8 Overall accuracy for coloured digital photograph from scale values of 81 to 85

Scale	Merge	Segmented Image	Classified Image	Overall Accuracy
81	90			78.57%

82	90			79.41%
83	90			80.00%
84	90			75.00%

| 85 | 90 | | | 72.36% |

The algorithm used for segmentation is edge-based algorithm, whereas for merging full-lambda schedule algorithm is used. Smaller the scale, smaller will be the segments, whereas bigger the scale, larger would be the segments. Smaller segments are appropriate for small objects like trees. Larger segments are appropriate for large objects such as roofs and road. An attempt was made to get an optimal scale and merge value where all the objects were segmented and classified at fine overall accuracy.

Results for individual objects/classes

As the scale values from 81 to 85 gives highest values of overall accuracy. Hence, we examine user's accuracy of each class/object at this range. On examining the values it is seen that tree is best extracted at scale 82 and merge 90 values with 85.71% user's accuracy. Road was extracted with quite good user's accuracy for all scale ranges with 100% overall accuracy at scale 81 and 82. Scale of 83 was able to provide best results for vegetation with 92.31% accuracy. Scale of 82 was found to be optimum for bare soil and red roof with 90.00% and 80.00% user's accuracy respectively. The highest accuracy was obtained at scale 83 for concrete roof and grey roof of 82.61% and 80.00% overall accuracy respectively.

Table 6-9 User's accuracy of each class for coloured digital photograph from scale values of 81 to 85

S.no	Scale	Merge	Tree	Road	Vegetation	Bare Soil	Red Roof	Concrete Roof	Grey Roof
1	81	90	75.00%	100%	81.48%	75.00%	60.00%	71.43%	62.50%
2	82	90	85.71%	100%	74.07%	90.00%	80.00%	68.18%	64.00%
3	83	90	70.83%	92.59%	92.31%	73.91%	70.00%	82.61%	80.00%
4	84	90	75.00%	92.59%	67.86%	69.57%	73.33%	69.57%	75.00%
5	85	90	66.67%	92.59%	75.00%	70.59%	75.00%	68.42%	56.00%

Again, individual accuracy was checked for each class from scale value of 81 to 85 as depicted in table 6-7. The optimal scale value for extraction of each class is summarized in table 6-8.
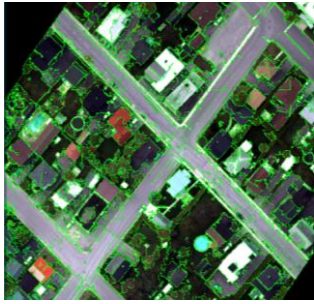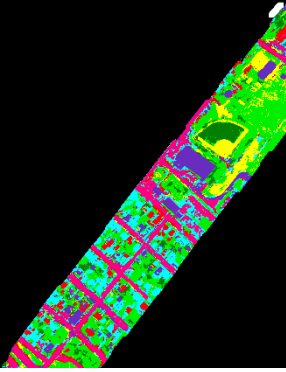
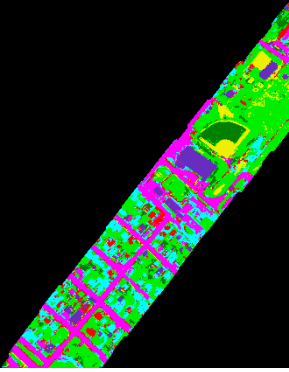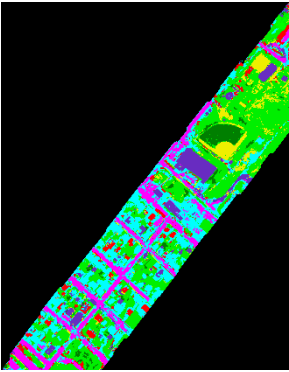Table 6-10 Optimum scale values for each class for coloured digital photograph
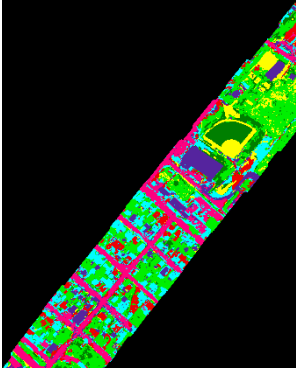
S.NO	CLASS	SCALE VALUE	MERGE VALUE
1	TREE	82	90
2	ROAD	81 and 82	90
3	VEGETATION	81	90
4	BARE SOIL	82	90
5	RED ROOF	82	90
6	CONCRETE ROOF	83	90
7	GREY ROOF	83	90

6.2.2. RESULTS FOR THE COMBINATION OF AIRBORNE LWIR HYPERSPECTRAL DATA WITH COLOURED DIGITAL PHOTOGRAPH

The thermal bands were added to the coloured digital photograph and subjected to object-oriented classification. The first step before classification is segmentation and merging process. The scale values are randomly chosen as 50, 60. 70, and 80. The merge value is set at 90 for all the scale values. The results are compiled in table 6-9. As the scale value increases, overall accuracy increases till 80. The algorithm used for segmentation is edge-based algorithm, whereas for merging full-lambda schedule algorithm is used. Smaller the scale, smaller will be the segments, whereas bigger the scale, larger would be the segments. Smaller segments are appropriate for small objects like trees. Larger segments are appropriate for large objects such as roofs and road. An attempt was made to get an optimal scale and merge value where all the objects were segmented and classified at fine overall accuracy.
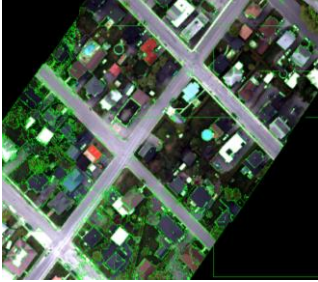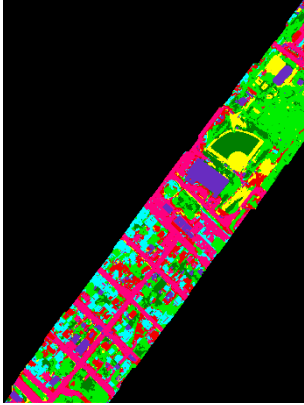
Table 6-11 Overall accuracy for combination of coloured digital photograph with thermal data from scale values 50 to 80
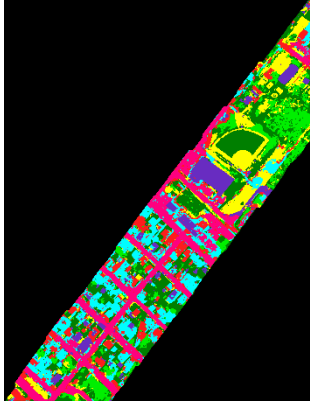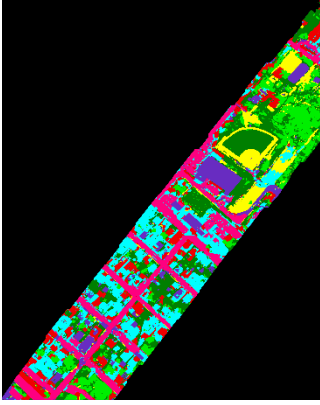
Scale	Merge	Segmented Image	Classified Image	Overall Accuracy
50	90			61.43%

60	90			65%
70	90			70%
80	90			80%

As the overall accuracy was highest at 80, hence scale values were tested from 81 to 85 for highest overall accuracy. The results are compiled in table 6-10. It was observed that highest overall accuracy was obtained for scale values of 82 and merge value of 90. The accuracy starts decreasing from 83 to 85 scale values.

Table 6-12 Overall accuracy for combination of coloured digital photograph with thermal data from scale values of 81 to 85

Scale	Merge	Segmented Image	Classified Image	Overall Accuracy
81	90			80.74%
82	90			85.71%
83	90			78.57%

84	90			77.78%
85	90			73.42%

Results for individual objects/classes

Now the best scale value was find out at which each object/class was extracted for scale 81 to 85 as shown in table 6-11. For tree overall accuracy of 85.71% was obtained at scale 82. For road two scale values were giving highest accuracy of 100.00% and 85.71% overall accuracy for v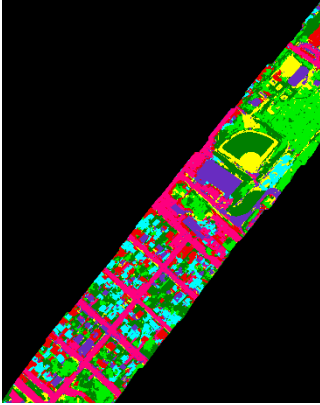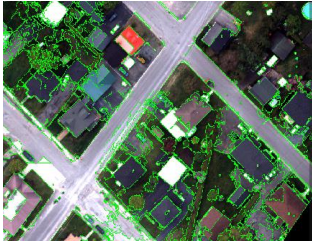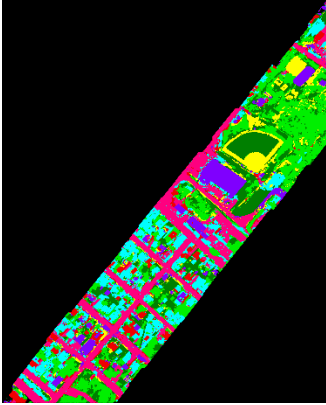egetation at scale 81 and highest accuracy of 76.41% was obtained for bare soil and 80.00% for red roof at scale 85. Concrete roof gave best results of 100.00% overall accuracy at scale 85. Whereas, grey roof gave 83.33% overall accuracy at scale 82. The optimal scale value for extraction of each class is summarized in table 6-12.

Table 6-13 User's accuracy of each class for combination of coloured digital photograph with thermal data from scale values of 81 to 85

S.no	Scale	Merge	Tree	Road	Vegetation	Bare Soil	Red Roof	Concrete Roof	Grey Roof
1	81	90	71.88%	96.55%	85.71%	75.00%	65.22%	95.00%	75.00%
2	82	90	85.71%	96.15%	82.35%	76.47%	80.00%	90.48%	83.33%
3	83	90	76.92%	85.19%	72.00%	75.00%	77.78%	93.33%	72.00%

| 4 | 84 | 90 | 72.73 % | 100.00 % | 78.57% | 60.00 % | 64.29 % | 94.74% | 64.00 % |
| 5 | 85 | 90 | 61.29 % | 100.00 % | 74.29% | 55.56 % | 76.92 % | 100.00% | 64.71 % |

Table 6-14 Optimum scale values for each class for combination of coloured digital photograph with thermal data

S.NO	CLASS	SCALE VALUE	MERGE VALUE
1	TREE	82	90
2	ROAD	84 and 85	90
3	VEGETATION	81	90
4	BARE SOIL	82	90
5	RED ROOF	82	90
6	CONCRETE ROOF	85	90
7	GREY ROOF	82	90

The best results for both the datasets i.e. coloured digital photograph and the combination of coloured digital photograph with thermal data are shown in figure 6-5 and 6-6 respectively.
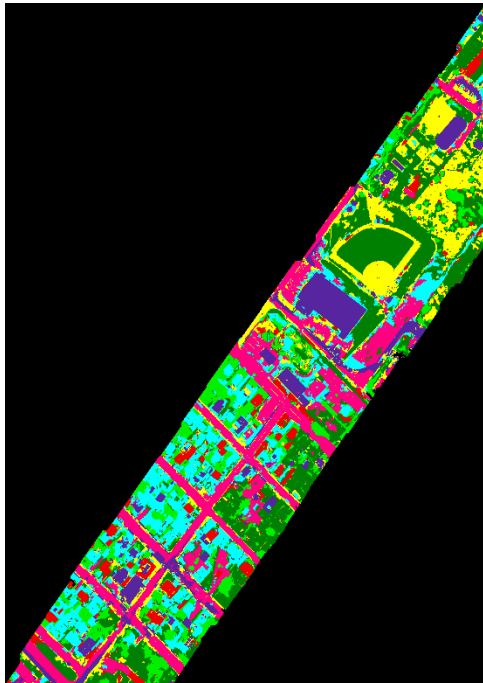
Figure 6-7 Land-cover map using SVM (Linear kernel) for coloured digital photograph
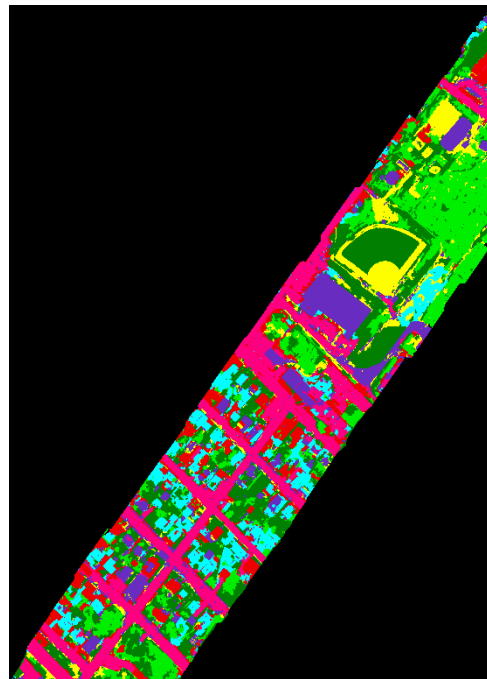
Figure 6-8 Land-cover map using SVM for combination of thermal data with coloured-digital photograph

6.2.3. RESULTS FOR ASTER THERMAL DATA

The object-oriented classification technique was also tested for multispectral thermal data i.e. ASTER thermal bands. Various scale and merge values were tested for this data. The best result was found to be for scale value of 50 and merge value of 10. The classified image is shown in figure 6-8. The legend is given in table 6-16. The classification was performed using support vector machine (SVM) with linear kernel. The overall accuracy was found to be 81.22% and the kappa coefficient was observed to be 0.6715. The performance of the five objects i.e. forest, agriculture, urban, sand and water was determined by comparing their user's accuracy. The compiled results of user's accuracy are given in table 6-15. Agriculture and sand were observed to be having high accuracy of 93.75% and 90.005 respectively. Urban area was mixed with forest at some locations. Water was found to be under-classified.

Table 6-15 User's accuracy for each class using object-oriented classification

SNO	CLASS	USERS ACCURACY
1	FOREST	84.21%
2	AGRICULTURE	93.75%
3	URBAN	65.12%
4	SAND	90.00%
5	WATER	75.00%

Overall accuracy = 81.22% and overall Kappa Statistics = 0.6715
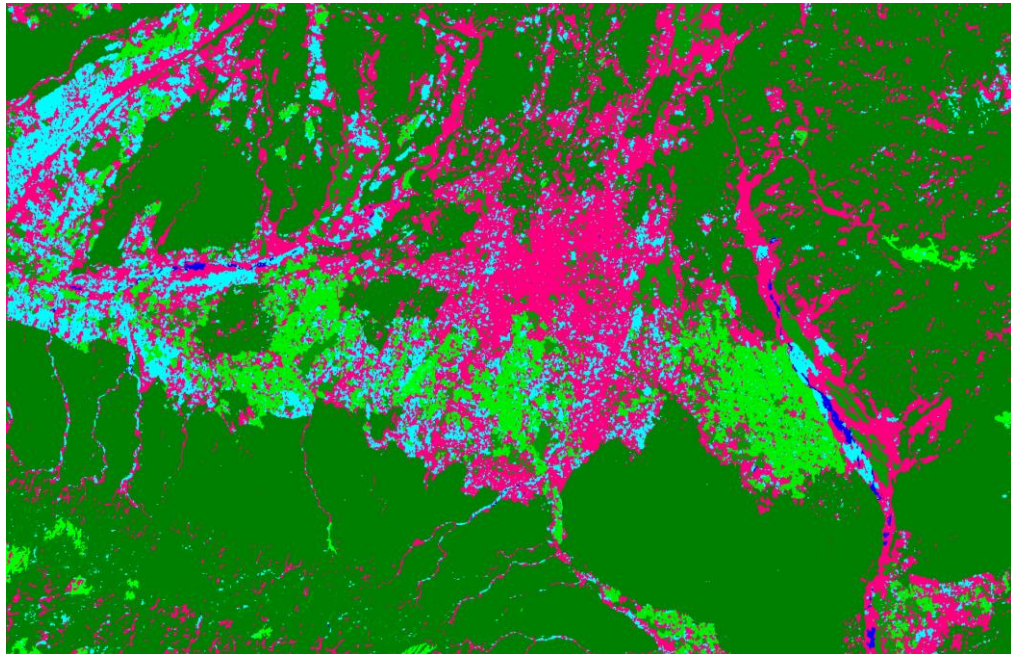
Figure 6-9 Classified image using object-oriented classification

Table 6-16 Legend

	Forest
	Agriculture
	Urban
	Water
	Sand

7. DISCUSSION

The key objective of this research work was to explore the potential of airborne thermal data for Landcover classification. The main aim of this section is to provide interpretations of the results obtained following the given methodology. The discussion is divided into three parts based on each of the objectives.

First objective deals with the application of minimum noise fraction (MNF) to airborne LWIR hyperspectral data and to the combination of thermal data with coloured digital photograph. MNF is a linear transformation. The Eigen values with respective gain in information is shown in figure 5-1. The bands that contains large eigen values contains data and the bands with less eigen values contains noise. The reduction in gain of information with increasing MNF components is shown in figure 5-2. According to the graph in figure 5-2, a saturation in values is noticed at MNF component equal to 7. Hence, seven MNF components are kept and given as input to classifiers.

Second objective concerns with the applicability of eight pixel-based classifiers for extraction of seven classes. All the classifiers are binary classifiers which detects the interest class and considers rest of the classes as background. Consequently, all the classes are combined together to form a Landcover map. Table 6-1 and 6-3 shows user accuracy for each of the seven class. With MNF, CEM and ACE provided highest accuracy for thermal data and combination of thermal data with coloured digital photograph respectively. In CEM misclassification is there in some of the roofs. As shown in figure 7-1 concrete roof is misclassified as bare soil. The reason for inefficiency of roof detection after observing the results of all the test sites and their analysis can be attributed roofs classified as bare soil or soil classified as roads. For ACE also a lot of misclassification exists in red roof and grey roof as shown in figure 7-2.
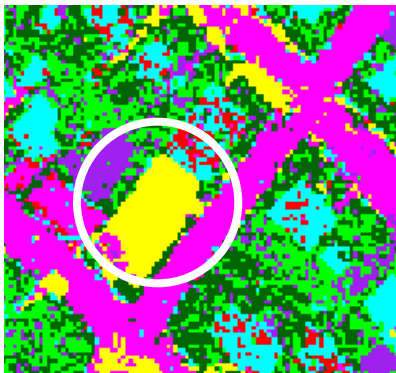
Figure 7-1 Misclassification using CEM algorithm with thermal data

Figure 7-2 Misclassification using ACE algorithm with combination of thermal data with coloured digital photograph

The area marked in white circle in these figures show a roof that missed detection. When MNF was not applied to the image before classification results were better. SAM classifier gave good results with high overall accuracy for both datasets. Spectral Angle Mapper (SAM) classifier uses an n-D angle to match target pixels to reference pixels. It determines the spectral similarity between target and reference pixels by calculating the angle between them. Smaller the angle closer the match to the reference pixel. Pixels more than the specified maximum angle threshold are left unclassified.

The pixel-based classification approach was also applied to ASTER thermal data. The classsifier chosen for thi spurpose was spectral angle mapper (SAM). This was chosen based on the performance of this classifier for airborne thermal hyperspectral data. The spatial resolution of ASTER thermal data is 90m, hence low angle value was found to be optimum for proper classification. The overall acuuracy obtained using this classifier for multispectral thermal data is 74.40%.
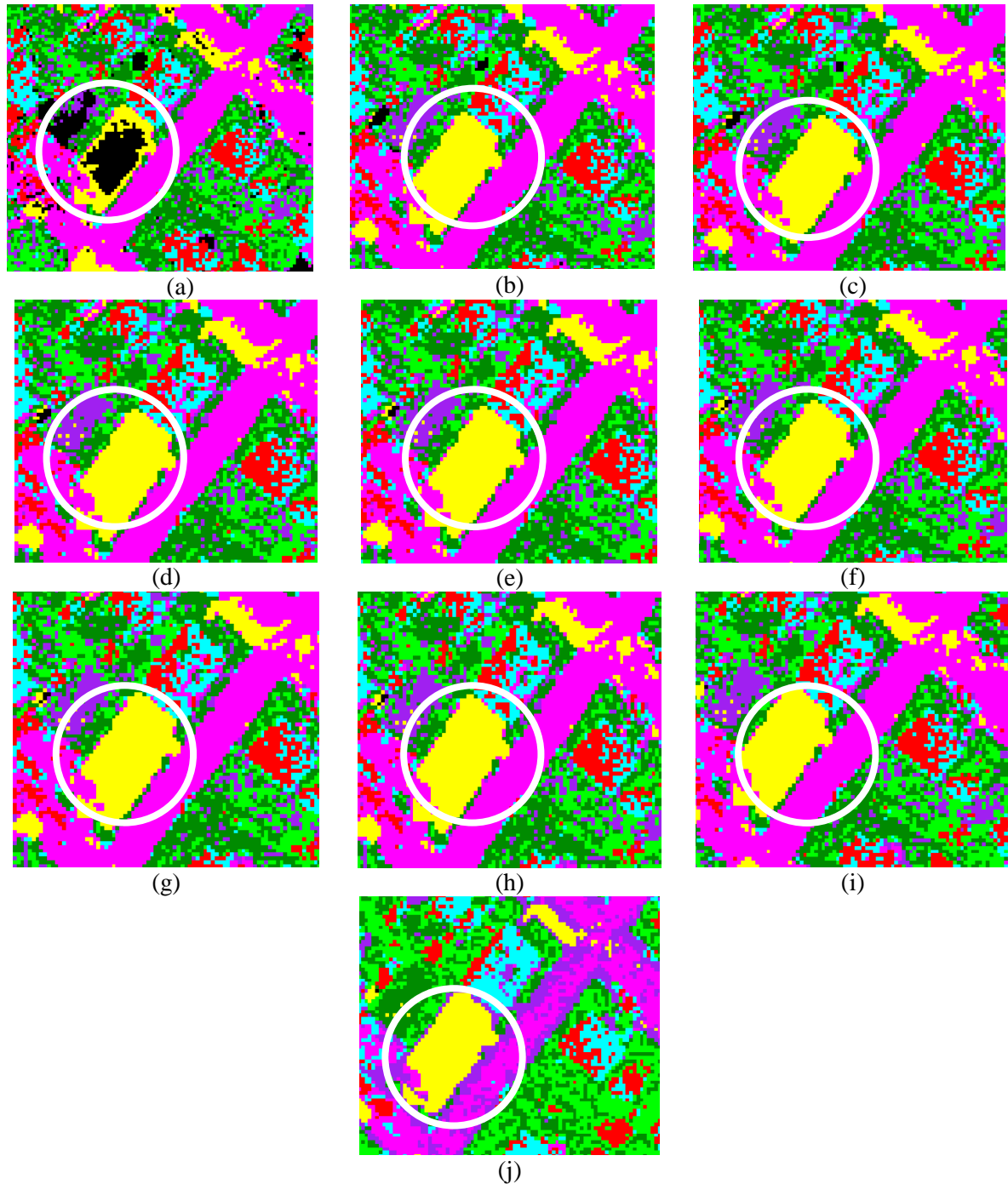
Figure 7-3 Effect of SAM angle on classification of thermal data: (a) At 0.01 radians; (b) At 0.02 radians; (c) At 0.03 radians; (d) At 0.04 radians; (e) At 0.05 radians; (f) At 0.06 radians; (g) At 0.07 radians; (h) At 0.08 radians; (i) At 0.09 radians; (j) At 0.01 radians.

Figure 7-3 shows a subset of the thermal image at various angle for SAM classifier. As can be seen from the figure 7-3(a) that unclassified pixels exists which occur in small angle of 0.01 radians. As we goes on increasing the angle unclassified pixels decreases. At 0.08 radians optimum value is reached with 81.71% overall accuracy. At angle greater than 0.08 radians misclassification starts. At 0.10 radians road is misclassified as concrete roof due to the similar brightness.

| (a) | (b) | (c) |
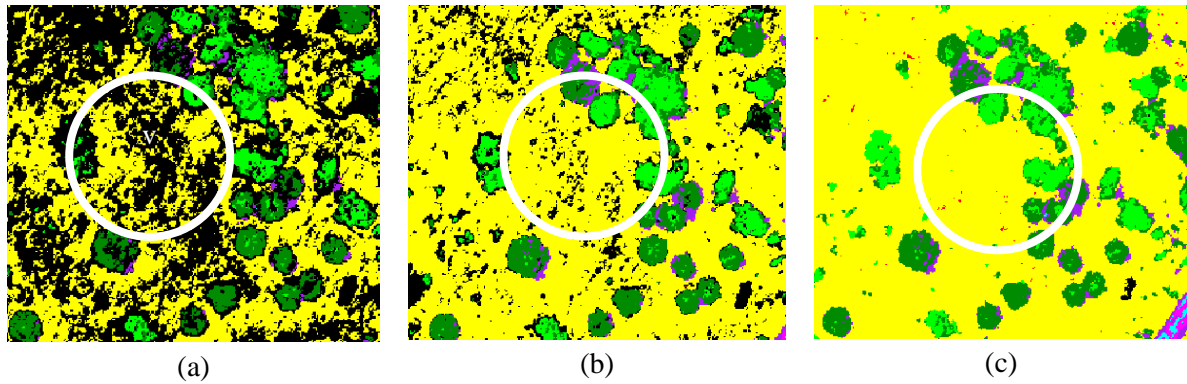
Figure 7-4 Effect of SAM angle on classification of combination of thermal data with coloured digital photograph: (a) At 0.01 radians; (b) At 0.06 radians; (c) At 0.08 radians.

The analysis for the combination of thermal data with coloured digital photograph is shown in figure--. The effect of angle is clearly seen on the classification results. Figure 7-4 (a) shows the result for angle 0.01 radians with highly unclassified object i.e. tree and bare soil. Figure 7-4 (b) and (c) shows improvement in classification results at angle 0.06, whereas the optimum angle is found at 0.08 radians.

Third objective in this study is application of object-oriented classification technique to the thermal data and the combination of thermal data with coloured digital photograph. Object-oriented classification is performed in two steps i.e. segmentation and classification. The effect of scale on the results of classification is checked. Scale values are checked in the order on increasing scale values from 50 to 80.

| (a) | (b) | (c) |
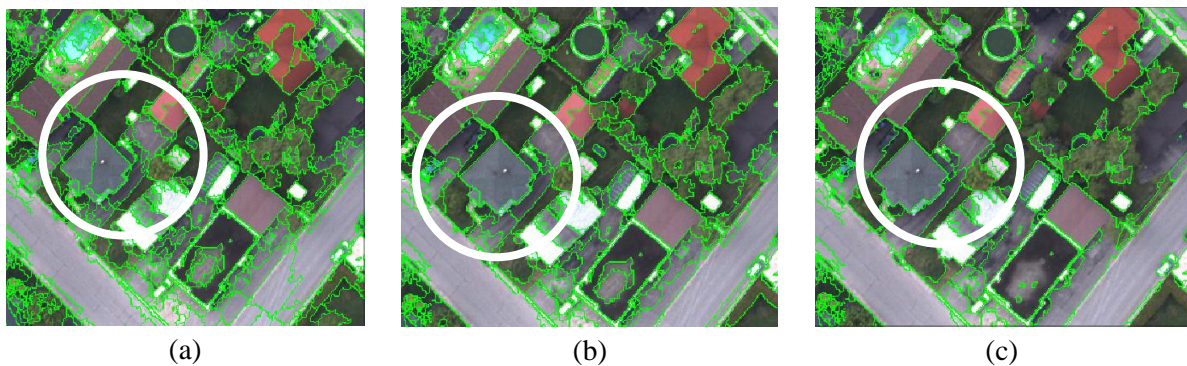
(d)

Figure 7-5 Effect of scale values on segmentation of coloured digital photograph: (a) At scale 50; (b) At scale 60; (c) At scale 70; (d) At scale 80.

At scale value of 50 and merge value of 90, smaller segments are generated as shown in figure 7-5 (a). The grey roof is segmented as one object when scale value of 60 is used as in figure 7-5 (b). At scale 70 red roof is merged to form an object as shown in figure 7-5 (c). At scale value of 80 and merge 90, all the roofs are distinctly visible as in figure 7-5 (d).

The object-oriented classification approach was also tested for ASTER thermal data. Various scale and merge values were tested. As the spatial resolution of thermal data is less i.e. 90m, hence small scale value was sufficient for segmentation. The segmentation was performed using scale value of 50 and merge value of 10. The overall accuracy obtained for multispectral thermla data is 81.22%. It is clear that object-oriented classification outperforms pixel-based classification for multispectral thermal data.

(a)

(b)

(c)
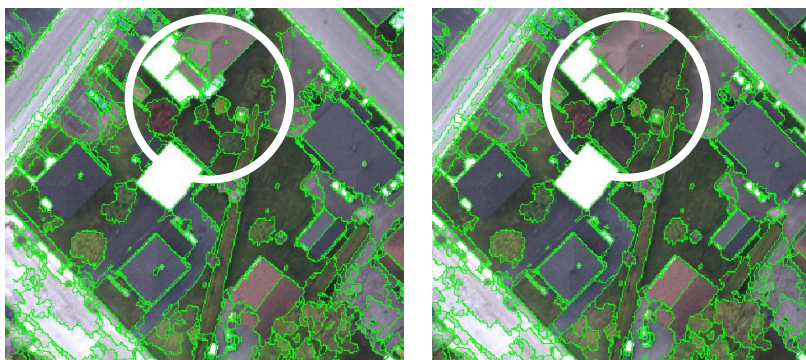
(d)

(e)

Figure 7-6 Effect segmentation of coloured digital photograph for fine tuning of scale value: (a) At scale 81; (b) At scale 82; (c) At scale 83; (d) At scale 84; (e) At scale 85.

The figure 7-6 shows the segmentation for scale value of 81 to 85. These scale values were tested for fine tuning of the scale. Hence, from figure 7-6 it is clear that scale value of 83 is found to be optimum. At scale 81 the number of segments are more, whereas at scale value of 85 various features are merged together.

The results for combination of coloured digital photograph with thermal data are compiled below.

(a)   (b)   (c)

(d)
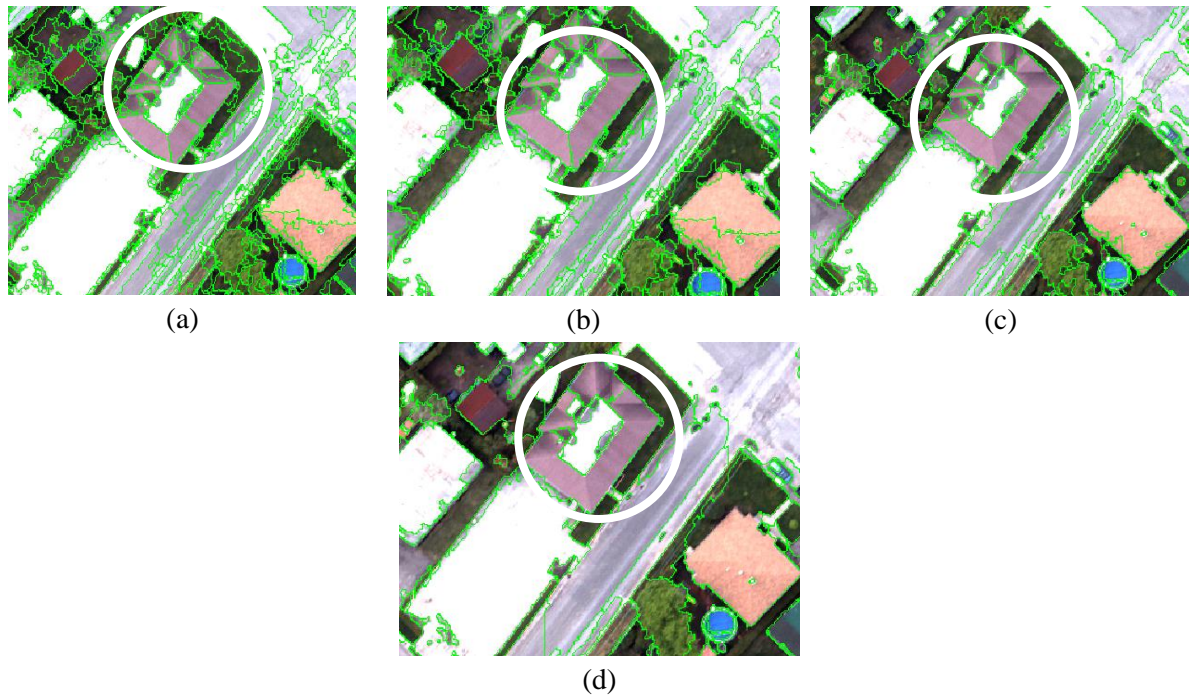
Figure 7-7 Effect of scale values on segmentation of combination of coloured digital photograph with thermal data: (a) At scale 50; (b) At scale 60; (c) At scale 70; (d) At scale 80.

The effect of scale on segmentation is clearly visible on the segmentation process in figure 7-7. As the scale is increasing number of segments are decreasing. For scale value of 50 and merge value of 90 the redo roof is divided into many segments. When the scale is reached to 80 red roof is identified or segmented properly as one object. The red roof is marked in white circle.

(a)   (b)   (c)

(d)   (e)
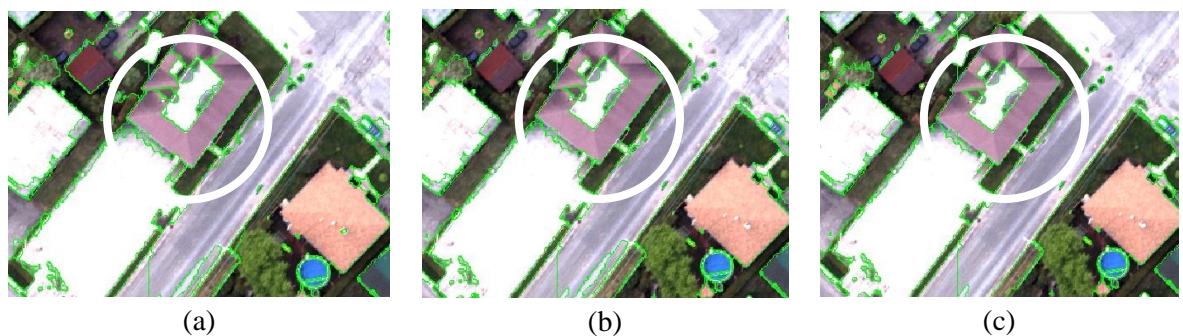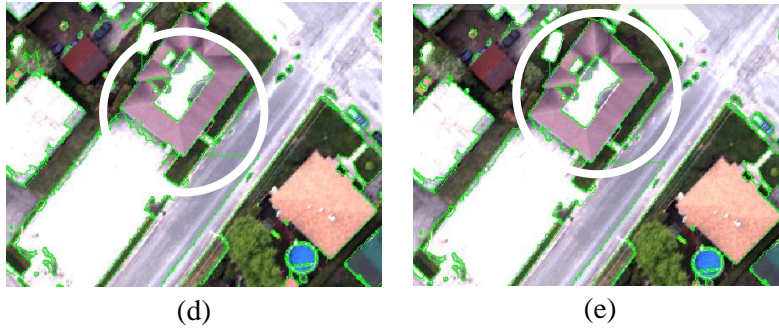
Figure 7-8 Effect segmentation of coloured digital photograph with thermal data for fine tuning of scale value: (a) At scale 81; (b) At scale 82; (c) At scale 83; (d) At scale 84; (e) At scale 85.

Now for the fine tuning of the scale, the values from 81 to 85 are analysed which are shown in figure 7-8. It is clear from the figure 7-8 (a) that at scale 81 number of segments are more which does not lead to good segmentation. At scale 82, the red roof in figure 7-8 (b) seems to be an optimum value as after this value there is not much change in the segmentation. In fact other objects starts merging.

Hence, it is clear that scale value plays a significant role in segmentation process. Smaller segmentation leads to over-segmentation, whereas large segments leads to under-segmentation. Segmentation also monitors the accuracy of classification. At last, it is evident that object-based image analysis approach was better than pixel-based approach for the classification purpose specifically for the various roofs. High spectral and spatial resolution of the given data offer challenges in mapping roofs. Concrete roofs, Red roofs and bright surfaces classes spectrally exhibit a great deal of confusion due to the similarity in material type. As we can observe from the results that the user accuracy for the roofs i.e. red roof, concrete roof and red roof are more than 60%. Here we can see that at higher scale values many of the objects are merges together to form one object. For example, roofs are merged together and trees are merged together. This may lead to under-segmentation which affects the classification accuracy.

There are numerous aspects that influences the accuracy of classification which includes: spectral resolution, spatial resolution of data, the reliability of training data chosen and the reference data provided, and the accuracy assessment method used. While the use of randomly selected field data points and error matrices has generally been acknowledged as a reliable means of conducting an accuracy assessment, this may not hold true with object-based classification. Object-based classification approach helps in removing the "salt-and-pepper" effect present in pixel-based classifications, may appear more visually appealing to the analyst, yet be under-evaluated by the single point/pixel and kappa index.

8. CONCLUSIONS AND RECOMMENDATIONS

8.1. CONCLUSION

This section provides the conclusion of the research work done based on the results gathered following the adopted methodology. The key objective is use of airborne LWIR hyperspectral data for Landcover classification. All the research objectives were successfully completed in this study. The research questions are as under:

➤ How MNF database will affect the results of object detection?

The MNF (minimum noise fraction) was applied to airborne hyperspectral data and the image was reduced to seven components. These MNF components were given as input to the pixel-based classifiers. The overall accuracy was calculated for each classifier. The hyperspectral data without MNF was also subjected to pixel-based classifiers and overall accuracy was calculated. The comparison of overall accuracy for thermal data is shown in table 6-2. It shows that accuracy increases if MNF is not applied to the thermal data. Application of MNF reduces the overall accuracy. The comparison of overall accuracy for the combination of thermal data with the coloured digital photograph is shown in table 6-4 showing decrease of accuracy after application of MNF to the combination of thermal data with coloured digital photograph.

➤ Which pixel-based classifier is best for extraction of each class?

Pixel-based classifiers were applied to two datasets i.e. to thermal data and to the combination of thermal data with coloured digital photograph. The comparison of user accuracy for each of the seven class is depicted in table 6-1 and 6-3. It is evident that pixel-based classification is still quite successful in classifying land cover of a homogenous nature (i.e. tree, road and vegetation). Pixel-based classification techniques do misclassify various pixels, mostly in land covers that are spectrally heterogeneous, such as various types of roof materials such as reed roof, concrete roof and grey roof. Spectral angle mapper (SAM) technique was found to be most suitable for extraction of each class for both the datasets as shown in table 6-2 and 6-4.

➤ Which object-based classifier is best-suited for extraction of each class?

Object-based classification was tested for two datasets i.e. coloured digital photograph and the combination of coloured digital photograph with thermal data. Various scale and merge values were examined for each dataset. The results for coloured digital photograph are shown in table 6-6 which suggests that scale value of 83 and merge value of 90 produced highest overall accuracy of 80%. Table 6-10 shows results for the combination of coloured digital photograph with the thermal data. The highest accuracy obtained is 85.71% or scale value of 82 and merge value of 90. The comparison of user accuracy for both datasets shows that object-oriented image analysis (OBIA) technique is quite successful in extraction of heterogeneous classes with almost more than 60% accuracy.

➤ Which approach is better: pixel-based or object-based technique?

On comparing the results of both pixel-based and object-based approaches it was found that object-oriented image analysis (OBIA) technique attain high individual producer's and user's accuracy for each

classified land cover class. This can be explained from the characteristics of both the classification methods. The visual difference between the classifications is quite evident. Also, it is witnessed that the results of pixel-based classification suffers from salt and pepper effect which is removed by using OBIA method. Object-oriented classification appears to overcome some of the problems encountered using pixel-based techniques to classify roof types and their characteristic spatial heterogeneity.

The eventual objective of this research work was to perform a comparison of detection algorithms based on statistical measure i.e. error (or confusion) matrix and to draw inferences from the algorithms that perform best. Pixel-based techniques and object-oriented image analysis approaches have been tested in this study. In object-oriented image analysis (OBIA), classification was performed on the group of pixels called objects. Proper segments created leads to fine classification in high spatial resolution imagery. The algorithm used for object-oriented classification was support vector machine (with linear kernel). SVM has given good results with linear kernel as data used is linearly separable. In pixel-based classification approach, with MNF as a pre-processing step the classifier with high performance was CEM i.e. constrained energy minimization algorithm and ACE i.e. adaptive coherence estimator. Also, when MNF was not used as a pre-processing step, SAM i.e. spectral angle mapper technique performed best. The main problem in pixel-based technique was that various roof types i.e. red roof, concrete roof and grey roofs were not detected using these techniques due to their spectral similarity and same roof material. This problem was solved using object-based technique. OBIA technique segmented the image based on area, length, spectral values etc. differentiating each roof. Then, SVM classification was performed which was quite successful in detecting these roof types with good user accuracy.

The object-oriented classification approach used in this paper provided results with an acceptable overall accuracy better than the pixel-based classification approach. This suggests that object-oriented analysis has great adequacy for extracting land cover information from remotely sensed image. This will be the situation especially with the expanding use of higher spatial and spectral resolution airborne imagery and the greater information it contains. It was clear from the results that pixel-based approaches were not efficient in identifying buildings. This was proven by the use of eight higher order pixel-based classifiers. Various scale and merge level were tested for identification of objects of different classes. It was found that there was no universally accepted method to determine optimal scale value for best accuracy. Also, a single scale value may not be appropriate for all the classes. The advantage of object-based classification approach is that various combination of parameters and attributes are available for class extraction. However, object-based approach is better than pixel-based approach for airborne LWIR hyperspectral data.

8.2. RECOMMENDATIONS

In this study pixel-based and object-based classification approach was tested for airborne LWIR hyperspectral data and ASTER thermal data. In pixel-based approach eight techniques were used, whereas for object-based technique SVM (with linear kernel) was used. A couple of suggestions have been included for future studies to upgrade the quality of the classification approach for landcover mapping.

➢ To improve the overall and user accuracies of the object-oriented classification, further work refining the process can be done. The use of multi-sensor data and ancillary data, such as derivative data sets and existing GIS layers, can be used.

➢ Another method with contextual information can be added for better extraction of objects while reducing noise.

➢ Future research can concentrate on attempts at improving the accuracy and efficiency incorporating thematic GIS layers or LIDAR data may enhance final product accuracy. These additional data layers have the potential to reduce classification confusion.

➢ To further limit the effects of different image characteristics, image pairs with similar illumination condition and view angles are preferred, if available.

➢ As a future recommendation this work can be improved by exploring more data dimensional approach such as kernel MNF. Further, thermal data can be converted into temperature and emissivity values for better extraction of classes.

LIST OF REFERENCES

Adar, S., Shkolnisky, Y., and Ben Dor, E., 2014. A new approach for thresholding spectral change detection using multispectral and hyperspectral image data, a case study over Sokolov, Czech republic. Int. J. Remote Sens. 35, 1563–1584. doi:10.1080/01431161.2013.878062

Anderson, J.R., Hardy, E.E., Roach, J.T., Witmer, R.E., and Peck, D.L., 1976. A Land Use And Land Cover Classification System For Use With Remote Sensor Data, A revision of the land use classification system as presented in U.S. Geological Survey Circular 671.

Bar, D.E., Wolowelsky, K., Swirski, Y., Figov, Z., Michaeli, A., Vaynzof, Y., and Abramovitz, Y., 2010. Target Detection and Verification via Airborne Hyperspectral and High-Resolution Imagery Processing and Fusion 10, 707–711.

Bioucas-dias, J.M., Plaza, A., Camps-valls, G., Scheunders, P., Nasrabadi, N.M., and Chanussot, J., 2013. Hyperspectral Remote Sensing Data Analysis and Future Challenges.

Birk, R.J., and McCord, T.B., 1994. Airborne hyperspectral sensor systems. Aerosp. Electron. Syst. Mag. IEEE 9, 26–33.

Boardman, J.W., and Kruse, F.A., 2011. Analysis of Imaging Spectrometer Data Using N -Dimensional Geometry and a Mixture-Tuned Matched Filtering Approach 49, 4138–4152.

Bochow, M., Heim, B., Kuster, T., Rogass, C., Bartsch, I., Segl, K., and Kaufmann, H., 2012. Automatic detection and delineation of surface water bodies in airborne hyperspectral data, in: Geoscience and Remote Sensing Symposium (IGARSS), 2012 IEEE International. IEEE, pp. 5226–5229.

Bongiovi, R.P., Hackwell, J.A., and Hayburst, T.L., 1998. Airborne LWIR hyperspectral measurements of military vehicles, in: Aerospace Applications Conference, 1996. Proceedings., 1996 IEEE. IEEE, pp. 121–135.

Brook, A., Ben-Dor, E., and Richter, R., 2010. Fusion of hyperspectral images and LiDAR data for civil engineering structure monitoring, in: Hyperspectral Image and Signal Processing: Evolution in Remote Sensing (WHISPERS), 2010 2nd Workshop on. IEEE, pp. 1–5.

Brown, A.J., 2006. Spectral curve fitting for automatic hyperspectral data analysis. IEEE Trans. Geosci. Remote Sens. 44, 1601–1608. doi:10.1109/TGRS.2006.870435

Chang, C., Schultz, R.C., Hobbs, M.C., Chen, S., Wang, Y., and Liu, C., 2015. Progressive Band Processing of Constrained Energy Minimization for Subpixel Detection. IEEE Trans. Geosci. Remote Sens. 53, 1626–1637. doi:10.1109/TGRS.2014.2346479

Chen, J., Jia, X., Yang, W., and Matsushita, B., 2009. Generalization of subpixel analysis for hyperspectral data with flexibility in spectral similarity measures. IEEE Trans. Geosci. Remote Sens. 47, 2165–2171. doi:10.1109/TGRS.2008.2011432

Cho, M.A., Mathieu, R., and Debba, P., 2009. Multiple endmember spectral-angle-mapper (SAM) analysis improves discrimination of savanna tree species, in: Hyperspectral Image and Signal Processing: Evolution in Remote Sensing, 2009. WHISPERS'09. First Workshop on. IEEE, pp. 1–4.

Dai, C., Huang, X., and Dong, G., 2007. Support Vector Machine for Classification of Hyperspectral Remote Sensing Imagery, in: Fourth International Conference on Fuzzy Systems and Knowledge Discovery, 2007. FSKD 2007. IEEE, Haikou, pp. 77 – 80. doi:10.1109/FSKD.2007.550

Darwish, A., Leukert, K., and Reinhardt, W., 2003. Image Segmentation for the Purpose Of Object-Based Classification, in: Geoscience and Remote Sensing Symposium, 2003. IGARSS '03. Proceedings. 2003 IEEE International. IEEE, pp. 2039 – 2041. doi:10.1109/IGARSS.2003.1294332

Du, B., and Zhang, L., 2014. Target detection based on a dynamic subspace. Pattern Recognit. 47, 344–358. doi:10.1016/j.patcog.2013.07.005

Du, B., Zhang, L., Tao, D., and Zhang, D., 2013. Unsupervised transfer learning for target detection from hyperspectral images. Neurocomputing 120, 72–82. doi:10.1016/j.neucom.2012.08.056

Du, P., Zhang, W., Zhang, S., and Xia, J., 2009. HYPERSPECTRAL REMOTE SENSING IMAGE CLASSIFICATION BASED ON DECISION LEVEL FUSION 940–943.

Du, Q., Ren, H., and Chang, C.I., 2003. A comparative study for orthogonal subspace projection and constrained energy minimization. IEEE Trans. Geosci. Remote Sens. 41, 1525–1529. doi:10.1109/TGRS.2003.813704

Du, Q., Ren, H., and Chang, C.-I., 2002. A study between orthogonal subspace projection and generalized likelihood ratio test in hyperspectral image analysis, in: Geoscience and Remote Sensing Symposium, 2002. IGARSS'02. 2002 IEEE International. IEEE, pp. 2575–2577.

Du, X., Chen, H., Liu, Z., Liu, M., and Cheng, X., 2013. Dimension Reduction for Hyperspectral image based on the Second Generation Bandelet Transform. Int. Symp. Photoelectron. Detect. Imaging 2013 Imaging Spectrom. Technol. Appl. 8910, 1–8. doi:10.1117/12.2032800

Duan, D., Shi, Y., Sun, L., and Wang, G., 2012. Remote sensing technology's applied research and development direction in Land-Use and Land-Cover Change (LUCC), in: 2012 2nd International Conference on Remote Sensing, Environment and Transportation Engineering, RSETE 2012 - Proceedings. IEEE, Nanjing, pp. 12–15. doi:10.1109/RSETE.2012.6260681

Duan, Y., Yan, L., and Jing, X., 2013. A novel method of destriping for airborne hyperspectral image, in: Geoscience and Remote Sensing Symposium (IGARSS), 2013 IEEE International. IEEE, pp. 4447–4450.

Foy, B.R., Petrin, R.R., Quick Jr, C.R., Shimada, T., and Tiee, J.J., 2002. Comparisons between hyperspectral passive and multispectral active sensor measurements, in: AeroSense 2002. International Society for Optics and Photonics, pp. 98–109.

Gao, S., Cheng, Y., Zhao, Y., Pan, Q., and Wu, Y., 2009. Multispectral infrared image for target detection based on matched filtering using tensor, in: Udupa, J.K., Sang, N., Nyul, L.G., Tong, H. (Eds.), . p. 74942C–74942C–7. doi:10.1117/12.832454

Gao, W., Zhang, X., Liu, Z.X., Lei, Y., Liu H., 2010. An improved Sobel edge detection, in: 3rd IEEE International Conference on Computer Science and Information Technology (ICCSIT), 2010. IEEE, Chengdu, pp. 67–71. doi:10.1109/ICCSIT.2010.5563693

Gao, Y., Mas, J.F., Niemeyer, I., Marpu, P.R., and Palacio, J.L., 2003. Object-based image analysis for mapping land-cover in a forest area, in: Proceedings from the 5th International Symposium on Spatial Data Quality. Enschede, The Netherlands, pp. 13–15.

Goetz, A.F.H., 2009. Remote Sensing of Environment Three decades of hyperspectral remote sensing of the Earth : A personal view. Remote Sens. Environ. 113, S5–S16. doi:10.1016/j.rse.2007.12.014

Govender, M., Chetty, K., and Bulcock, H., 2007. A review of hyperspectral remote sensing and its application in vegetation and water resource studies. Water Sa 33.

Graham, S., 1999. Remote Sensing : Feature Articles [WWW Document]. URL http://earthobservatory.nasa.gov/Features/RemoteSensing/ (accessed 6.8.15).

Haavardsholm, T. V, Arisholm, G., Kavara, A., and Skauli, T., 2010. Architecture of the real-time target detection processing in an airborne hyperspectral demonstrater system 1–4.

Ji, A., Pang, J., Li, S., and Sun, J., 2006. Support vector machine for classification based on fuzzy training data, in: International Conference on Machine Learning and Cybernetics, 2006. IEEE, Dalian, China, pp. 13–16. doi:10.1109/ICMLC.2006.258838

Jin, X., Paswaters, S., and Cline, H., 2009. A comparative study of target detection algorithms for hyperspectral imagery. Proc. SPIE 7334, Algorithms Technol. Multispectral, Hyperspectral, Ultraspectral Imag. XV 7334, 73341W–73341W–12. doi:10.1117/12.818790

JPL, N., 2004. ASTER User Handbook 135.

Kaewpijit, S., Le Moigne, J., and El-Ghazawi, T., 2002. Spectral data reduction via wavelet decomposition, in: AeroSense 2002. International Society for Optics and Photonics, pp. 56–63.

Kaganami, H.G., and Beiji, Z., 2009. Region-based segmentation versus edge detection. IIH-MSP 2009 - 2009 5th Int. Conf. Intell. Inf. Hiding Multimed. Signal Process. 1217–1221. doi:10.1109/IIH-MSP.2009.13

Kasen, I., Goa, P.E., and Skauli, T., 2004. Target detection in hyperspectral images based on multicomponent statistical models for representation of background clutter, in: Driggers, R.G., Huckridge, D.A. (Eds.), . pp. 258–264. doi:10.1117/12.578782

Khan, A., Kim, I., and Kong, S.G., 2009. Dimensionality Reduction of Hyperspectral Images using Kernel ICA 7315, 1–8. doi:10.1117/12.820004

Kirkland, L., Herr, K., Keim, E., Adams, P., Salisbury, J., Hackwell, J., and Treiman, A., 2002. First use of an airborne thermal infrared hyperspectral scanner for compositional mapping. Remote Sens. Environ. 80, 447–459.

Kumar, U., 2006. Comparative Evaluation of the Algorithms for Land Cover Mapping using Hyperspectral Data. International Institute for Geo-information Science and Earth Observation Enschede, Netherlands, Indian Institute of Remote Sensing.

Kupková, L., Potůčková, M., Kopalová, I., and Kolář, J., 2009. Object Based Image Analysis for Urbanized Areas, in: Proceedings of the 29th Symposium of the European Association of Remote Sensing Laboratories. Chania, Greece, pp. 231–240.

Kwon, H., and Nasrabadi, N.M., 2007. Kernel spectral matched filter for hyperspectral imagery. Int. J. Comput. Vis. 71, 127–141. doi:10.1007/s11263-006-6689-3

Lennon, M., Mercier, G., Mouchot, M.-C., and Hubert-Moy, L., 2002. Curvilinear component analysis for nonlinear dimensionality reduction of hyperspectral images, in: Proc. SPIE 4541. Toulouse, France, pp. 157–168. doi:10.1117/12.454150

Li, H., Sun, G., Sun, H., and Liu, W., 2012. Watershed Algorithm Based on Morphology for Dental X-Ray Images Segmentation, in: IEEE 11th International Conference on Signal Processing (ICSP), 2012 (Volume:2). IEEE, Beijing, pp. 877 – 880. doi:10.1109/ICoSP.2012.6491720

Li, W., Tramel, E.W., Prasad, S., Fowler, J.E., and Member, S., 2014. Nearest Regularized Subspace for Hyperspectral Classification 52, 477–489.

Liew, S.C., 2001. Principles of Remote Sensing - Centre for Remote Imaging, Sensing and Processing, CRISP [WWW Document]. Interpret. Opt. Remote Sens. Images. URL www.crisp.nus.edu.sg (accessed 6.8.15).

Liu, X., and Yang, C., 2013. School of Computer Science, Sichuan University of Science and Engineering, Zigong, China, in: Image and Signal Processing (CISP), 2013 6th International Congress on. IEEE, pp. 814–818.

Lopez-Molina, C., Bustince, H., Barrenechea, E., Jurio, A., and De Baets, B., 2011. Multiscale edge detection based on the Sobel method, in: International Conference on Intelligent Systems Design and Applications, ISDA. IEEE, Cordoba, pp. 666–671. doi:10.1109/ISDA.2011.6121732

Luo, W., Zhong, L., Zhang, B., and Luo, S., 2007. Analysis on hyperspectral target detection ability and target feature in 6787, 1–8. doi:10.1117/12.747827

Ma, Y., Fang, T., Fang, K., Wang, D., and Che, W., 2002. Texture image classification based on support vector machine and distance classification, in: World Congress on Intelligent Control and Automation. IEEE, pp. 551–554. doi:10.1109/WCICA.2002.1022171

MacDonald, J.S., Ustin, S.L., and Schaepman, M.E., 2009. The contributions of Dr. Alexander F.H. Goetz to imaging spectrometry. Remote Sens. Environ. 113, S2–S4. doi:10.1016/j.rse.2008.10.017

Manolakis, dimitris, Lockwood, R., Cooley, T., and Jacobson, J., 2007. Robust matched filters for target detection in hyperspectral imaging data 529–532.

Men, H.M.H., Gao, Y.G.Y., Wu, Y.W.Y., and Li, X.L.X., 2009. Study on Classification Method Based on Support Vector Machine, in: 2009 First International Workshop on Education Technology and Computer Science. IEEE, Wuhan, Hubei, pp. 369–373. doi:10.1109/ETCS.2009.344

Mozaffar, M.H., Zoej, M.J.V., Sahebi, M.R., and Rezaei, Y., 2008. Vegtation endmember extraction in Hyperion images. Int. Arch. oj Photogramm. Remote Sens. Spat. Sci. 37, 409–412.

Nand, N., and Kumar, K., 1989. The Holy Himalaya: A Geographical Interpretation of Garhwal. Daya Books.

Ng, H.P., Ong, S.H., Foong, K.W.C., Goh, P.S., and Nowinski, W.L., 2006. Medical Image Segmentation Using K-Means Clustering and Improved Watershed Algorithm, in: 2006 IEEE

Southwest Symposium on Image Analysis and Interpretation. IEEE, Denver, CO, pp. 61–65. doi:10.1109/SSIAI.2006.1633722

Olmanson, L.G., Brezonik, P.L., and Bauer, M.E., 2013. Remote Sensing of Environment Airborne hyperspectral remote sensing to assess spatial distribution of water quality characteristics in large rivers : The Mississippi River and its tributaries in Minnesota. Remote Sens. Environ. 130, 254–265. doi:10.1016/j.rse.2012.11.023

Project, P., Pickering, V., Yorks, N., and Caldwell, A.E., 2000. The application of remote sensing in archaeology : a study of crop mark detection using airborne thermal infrared imagery in the Heslerton 4131, 185–193.

Racek, F., and Baláž, T., 2012. Spectral Angle Mapper as a Tool for Matching the Spectra in Hyperspectral Processing. Univ. Def. 65.

Rafiee, A., and Saradjian, M.R., 2008. Classification of Buildings and Roads Using Support Vector Machine, in: Digital Image Computing: Techniques and Applications (DICTA), 2008. IEEE, Canberra; ACT, pp. 111 – 116. doi:10.1109/DICTA.2008.57

Ratches, J.A., 2011. Review of current aided∕automatic target acquisition technology for military target acquisition tasks. Opt. Eng. doi:10.1117/1.3601879

Ratches, J.A., Vollmerhausen, R.H., and Driggers, R.G., 2001. Target Acquisition Performance Modeling of Infrared Imaging Systems: Past, Present, and Future. Sensors Journal, IEEE 1, 31–40. doi:10.1109/JSEN.2001.923585

Ren, H., and Chang, C.-I., 2000. A target-constrained interference-minimized filter for subpixel target detection in hyperspectral imagery, in: Geoscience and Remote Sensing Symposium, 2000. Proceedings. IGARSS 2000. IEEE 2000 International. IEEE, pp. 1545–1547.

Ren, H., Du, Q., Chang, C.-I., and Jensen, J.O., 2003. Comparison between constrained energy minimization based approaches for hyperspectral imagery, in: Advances in Techniques for Analysis of Remotely Sensed Data, 2003 IEEE Workshop on. IEEE, pp. 244–248.

Salehi, B., Zhang, Y., and Zhong, M., 2011. Combination of object-based and pixel-based image analysis for classification of vhr imagery over urban areas. Am. Soc. Photogramm. Remote Sens. Annu. Conf. 2011 454–460.

Shackelford, A.K., and Davis, C.H., 2003. A combined fuzzy pixel-based and object-based approach for classification of high-resolution multispectral data over urban areas. IEEE Trans. Geosci. Remote Sens. 41, 2354–2363. doi:10.1109/TGRS.2003.815972

Shahshahani, B.M., and Landgrebe, D.A., 1994. The Effect of Unlabeled Samples in Reducing the Small Sample Size Problem and Mitigating the Hughes Phenomenon 3.

Shaw, G.A., and Burke, H.K., 2003. Spectral imaging for remote sensing. Lincoln Lab. J. 14, 3–28.

Shi, Z., Yang, S., and Jiang, Z., 2013. Target detection using difference measured function based matched filter for hyperspectral imagery. Opt. - Int. J. Light Electron Opt. 124, 3017–3021. doi:10.1016/j.ijleo.2012.09.003

Short, N.M., 2005. Remote Sensing Tutorial [WWW Document]. URL http://fas.org/irp/imint/docs/rst/Sect13/Sect13_5.html (accessed 5.21.15).

Sigernes, F., 1996. Airborne Hyperspectral Imaging. Univ. Cent. SVALBARD 1–17.

Sims, F.M., and Mesev, V., 2007. Use of Ancillary Data in Object Based Classification of High Resolution Satellite Data, in: 2007 Urban Remote Sensing Joint Event. IEEE, Paris, pp. 1 – 10. doi:10.1109/URS.2007.371824

Singh, P., and Singh, S., 2011. Landuse Pattern Analysis Using Remote Sensing : A Case Study of Mau District , India. Arch. Appl. Sci. Res. 3, 10–16.

Small, G.W., and Zhang, L., 2002. Data analysis strategies for passive multispectral and hyperspectral infrared remote sensors, in: Environmental and Industrial Sensing. International Society for Optics and Photonics, pp. 115–126. doi:10.1117/12.455728

Teke, M., Deveci, H.S., Haliloglu, O., Gurbuz, S.Z., and Sakarya, U., 2013. A short survey of hyperspectral remote sensing applications in agriculture, in: Recent Advances in Space Technologies (RAST), 2013 6th International Conference on. IEEE, pp. 171–176.

The 2014 IEEE GRSS Data Fusion contest: description of the datasets, 2014.

Tiwari, K.C., Arora, M.K., Singh, D., and Yadav, D., 2013. Military target detection using spectrally modeled algorithms and independent component analysis. Opt. Eng. 52, 026402–026402.

Tsai, Y.H., Stow, D., and Weeks, J., 2011. Comparison of object-based image analysis approaches to mapping new buildings in Accra, Ghana using multi-temporal quickbird satellite imagery. Remote Sens. 3, 2707–2726. doi:10.3390/rs3122707

Vane, G., and Goetz, A.F., 1985. Imaging Spectrometer Data Analysis Workshop.

Wang, T., Du, B., and Zhang, L., 2013. A kernel-based target-constrained interference-minimized filter for hyperspectral sub-pixel target detection. IEEE J. Sel. Top. Appl. Earth Obs. Remote Sens. 6, 626–637. doi:10.1109/JSTARS.2013.2251863

Wang, Y., Huang, S., Liu, D., and Wang, B., 2012. Research Advance on Band Selection-based Dimension Reduction of Hyperspectral Remote Sensing Images 1–4.

Wilson, T.L., and Davis, C.O., 1998. Hyperspectral remote sensing technology (HRST) program and the Naval EarthMap Observer (NEMO) satellite, in: SPIE's International Symposium on Optical Science, Engineering, and Instrumentation. International Society for Optics and Photonics, pp. 2–10.

Winter, M.E., and Winter, E.M., 2002. Resolution enhancement of hyperspectral data, in: Aerospace Conference Proceedings, 2002. IEEE. IEEE, pp. 3–1523.

Wu, Y., Ke, Y., Gong, H., Chen, B., and Zhu, L., 2014. Comparison of object-based and pixel-based methods for urban land-use classification from WorldView-2 imagery, in: 2014 3rd International Workshop on Earth Observation and Remote Sensing Applications (EORSA). IEEE, Changsha, pp. 284 – 288. doi:10.1109/EORSA.2014.6927896

Xie, H., Tong, X., Heipke, C., Lohmann, P., and Sorgel, U., 2009. Object-based binary encoding algorithm-an integration of hyperspectral data and DSM, in: Urban Remote Sensing Event, 2009 Joint. IEEE, pp. 1–6.

Xin, W., Yi-ping, L., Ting, J., Hui, G., Sheng, L., and Xiao-wei, Z., 2011. A New Classification Method For LIDAR Data Based on Unbalanced Support Vector Machine, in: International Symposium on Image and Data Fusion (ISIDF), 2011. IEEE, Tengchong, Yunnan, pp. 1–4. doi:10.1109/ISIDF.2011.6024312

Xu, G., 2000. Basic research in the field of thermal infrared remote sensing. Sci. China Ser. E Technol. Sci. 43, 1–8. doi:10.1007/BF02916572

Yang, G.-P., Liu, H.-Y., and Yu, X.-C., 2007. Hyperspectral remote sensing image classification based on kernel fisher discriminant analysis, in: International Conference on Wavelet Analysis and Pattern Recognition, 2007. ICWAPR '07. IEEE, Beijing, China, pp. 1139–1143. doi:10.1109/ICWAPR.2007.4421604

Yang, H., Ma, B., Du, Q., and Yang, C., 2010. Improving urban land use and land cover classification from high-spatial-resolution hyperspectral imagery using contextual information. J. Appl. Remote Sens. 4, 041890. doi:10.1117/1.3491192

Yang, S., and Shi, Z., 2014. SparseCEM and SparseACE for Hyperspectral Image Target Detection 11, 2135–2139.

Yao, H., Hruska, Z., Kincaid, R., Ononye, A., and Brown, R.L., Cleveland, T.E., 2010. Spectral Angle Mapper classification of fluorescence hyperspectral image for aflatoxin contaminated corn, in: Hyperspectral Image and Signal Processing: Evolution in Remote Sensing (WHISPERS), 2010 2nd Workshop on. IEEE, pp. 1–4.

Ying, W.Y.W., Zelin, S.Z.S., and Haibin, Y.H.Y., 2003. Wavelet analysis based detection algorithm for infrared image small target in background of sea and sky, in: 3rd International Symposium on Image and Signal Processing and Analysis, 2003. ISPA 2003. Proceedings of the. IEEE, Orlando, FL, pp. 123–131. doi:10.1109/ISPA.2003.1296861

Yu, Q., Gong, P., Clinton, N., Biging, G., Kelly, M., and Schirokauer, D., 2006. Objectbased detailed vegetation classification with airborne high spatial resolution remote sensing imagery. Photogramm. Eng. Remote Sensing 72, 799–811. doi:10.14358/PERS.72.7.799

Zerrouki, N., and Bouchaffra, D., 2014. Pixel-Based or Object-Based : Which Approach is More Appropriate for Remote Sensing Image Classification ?, in: IEEE International Conference on Systems, Man and Cybernetics (SMC). IEEE, San Diego, CA, pp. 864–869. doi:10.1109/SMC.2014.6974020

Zhang, H., Zhu, Q., and Guan, X.F., 2012. Probe into image segmentation based on sobel operator and maximum entropy algorithm, in: Proceedings - 2012 International Conference on Computer Science and Service System, CSSS 2012. IEEE, Nanjing, pp. 238–241. doi:10.1109/CSSS.2012.67

Zhang, J., and Jia, L., 2014. A comparison of pixel-based and object-based land cover classification methods in an arid/semi-arid environment of Northwestern China, in: 2014 Third International Workshop on Earth Observation and Remote Sensing Applications (EORSA). IEEE, Changsha, pp. 403–407. doi:10.1109/EORSA.2014.6927922

Zhang, J., Ye, Z., and Zhou, T., 2001. Classification of hyperspectral data using support vector machine, in: International Conference on Image Processing, 2001. Proceedings. 2001 (Volume:1). IEEE, Thessaloniki, pp. 882–885. doi:10.1109/ICIP.2001.959187

Zhang, J., Zhang, W., Jiao, H., and Zhang, Y.E., 2008. Spaceborne hyperspectral image generation based on airborne hyperspectral image, in: IEEE International Geoscience and Remote Sensing Symposium, 2008. IGARSS 2008. (Volume:4). IEEE, Boston, MA, pp. 259–262. doi:10.1109/IGARSS.2008.4779707

Zhang, L., Zhang, L., Tao, D., and Huang, X., 2014. Sparse Transfer Manifold Embedding for Hyperspectral Target Detection. IEEE Trans. Geosci. Remote Sens. 52, 1030–1043. doi:10.1109/TGRS.2013.2246837

Zhang, L.Z.L., Frigui, H., Gader, P., and Bolton, J., 2009. Context-Dependent Fusion for mine detection using Airborne Hyperspectral Imagery, in: 2009 First Workshop on Hyperspectral Image and Signal Processing: Evolution in Remote Sensing. IEEE, Grenoble, pp. 1–4. doi:10.1109/WHISPERS.2009.5288973

Zhang, X., Chen, L., Pan, L., and Xiong, L., 2012. Study on the image segmentation based on ICA and watershed algorithm, in: Proceedings - 2012 5th International Conference on Intelligent Computation Technology and Automation, ICICTA 2012. IEEE, Zhangjiajie, Hunan, pp. 505–508. doi:10.1109/ICICTA.2012.132

Zhao, Y., Liu, J., Li, H., and Li, G., 2008. Improved watershed algorithm for dowels image segmentation, in: Proceedings of the World Congress on Intelligent Control and Automation (WCICA). IEEE, Chongqing, pp. 7640–7643. doi:10.1109/WCICA.2008.4594115

Zheng, L., Wan, L., Huo, H., and Fang, T., 2014. A Noise Removal Approach for Object-based Classification of VHR Imagery via Post-classification, in: 2014 International Conference on Audio, Language and Image Processing (ICALIP). IEEE, Shanghai, pp. 915–920. doi:10.1109/ICALIP.2014.7009928

Zhou, X., Tamas, J., Chen, C., and Verone, M.W., 2012. Urban Land Cover Mapping Based on Object Oriented Classification Using WorldView 2 Satellite Remote Sensing Images, in: International Scientific Conference on Sustainable Development & Ecological Footprint. Sopron, Hungary, pp. 26–27.

Zhu, F., Ye, N., Xu, S., and Gu, X., 2011. Support vectors classification and incremental learning, in: Proceedings - 2011 6th IEEE Joint International Information Technology and Artificial Intelligence Conference, ITAIC 2011. IEEE, Chongqing, pp. 206–210. doi:10.1109/ITAIC.2011.6030187

Zhu, J., Zhou, L., and Zhang, D., 2011. Identification for building surface material based on hyperspectral remote sensing, in: Proceedings - 2011 19th International Conference on Geoinformatics, Geoinformatics 2011. IEEE, Shanghai, pp. 1 – 5. doi:10.1109/GeoInformatics.2011.5980687

Zhuo, W., and Lili, C., 2010. The algorithm of text classification based on rough set and support vector machine, in: 2010 2nd International Conference on Future Computer and Communication. IEEE, Wuhan, pp. V1–365–V1–368. doi:10.1109/ICFCC.2010.5497769

APPENDIX

PUBLICATIONS

1. One publication in the International Archives of the Photogrammetry, Remote Sensing and Spatial Information Sciences, Volume XL-8, 2014, ISPRS Technical Commission VIII Symposium, 09 – 12 December 2014, Hyderabad, India. Titled "*Target detection algorithm for airborne thermal hyperspectral data*" (mini project work).
2. Other paper under review titled "*Object-Oriented and Pixel-Based Classification approach for Land-cover using airborne LWIR hyperspectral data*" in Journal of Applied Remote Sensing.